MODELING THE ISOMERIZATION OF LACTONES AND THE ROLE OF CATALYSTS IN HETERO-DIELS-ALDER REACTIONS

by

Büşra Dereli

B.S., Chemistry, Boğaziçi University, 2012

Submitted to the Institute for Graduate Studies in
Science and Engineering in partial fulfillment of
the requirements for the degree of
Master of Science

Graduate Program in Chemistry
Boğaziçi University
2013

To my family

ACKNOWLEDGEMENTS

I would like to express my sincere gratitude to my thesis advisor Prof. Viktorya Aviyente for her supervision, endless patience and assistance throughout my studies. It was a great opportunity to study in her group and improve myself thanks to her invaluable comments and excellent scientific guidance.

I truly appreciate the guidance of the members of my committee: Assoc. Prof. A. Neren Ökte (Boğaziçi University) and Assoc. Prof. Nurcan Tüzün (Istanbul Technical University). I'm thankful to Prof. İlknur Doğan for giving her valuable time and advices.

I would like to thank all the members of the Computational Chemistry Group, Tuğba Furuncuoğlu, Özlem Karahan, Gülşah Çifci, Sesil Agopcan, Gamze Bahadır, Tuğçe Erbay, İlke Uğur, Burcu Dedeoğlu, Deniz Akgül and Esra Bozkurt for their enjoyable company and valuable contributions to my studies. I wish to express my truly pleasure to Assist. Prof. F. Ahu Akın for her delightful conversations and advice lead me in my future career and in life. I would also like to thank all my friends and all the members of the Chemistry Department who were exactly like a family for me during these years.

Finally, my innermost thanks to my mother and father, and my friends who are also a part of my family, Ezgi Okur, İrem Tatar, Sedef Günday, Yeşim Hebip for their continuous support and endless love throughout my life.

ABSTRACT

MODELING THE ISOMERIZATION OF LACTONES AND THE ROLE OF CATALYSTS IN HETERO-DIELS-ALDER REACTIONS

In this study, the isomerization of a strigolactone analogue and the catalyst effect on the Hetero-Diels-Alder reactions is investigated by the quantum mechanical tools. In the first part, the interconversion of the strigolactone analogue between its E and Z isomers as well as the atropisomers in an effort to interpret the nature of the isomeric mixture is studied. Density functional theory calculations reveal that a mixture of E and Z isomers can exist concurrently as a result of being formed in the same environment. To the extent of barrier heights which can be surmounted at room temperature, E atropisomers render an affordable interconversion with lower activation energies. On the other hand, Z atropisomers display higher barriers which can be possibly overcome in time. In the second part, transition metal catalyst effect on 1,2-diazine and siloxy alkyne cycloaddition reactions is investigated. Silver(I) as a transition metal plays a crucial role in lowering the activation barriers of 1,2-diazine and siloxy alkyne cycloadditions, which otherwise require thermal conditions. Substitution effect on 1,2-diazine and siloxy alkyne is also taken into account. Relativistic density functional theory calculations prove that the primary role of a metal catalyst in an inverse electron demand Hetero-Diels-Alder reaction is to facilitate the overlap between HOMO of the dienophile and LUMO of the diene by reducing the energy gap. Elucidating the role of catalysis in the 1,2-diazine and siloxy alkyne cycloadditions under mild conditions, possible reaction mechanisms are proposed to shed light on the behavior of the hetero-Diels-Alder reaction.

ÖZET

LAKTON İZOMERİZASYONU VE HETERO-DİELS-ALDER TEPKİMELERİNDE KATALİZÖR ETKİSİNİN MODELLENMESİ

Bu çalışmada, strigolakton türevinin izomerizasyonu ve Hetero-Diels-Alder tepkimelerinde katalizör etkisi incelenmiştir. Birinci kısımda, strigolakton türevinin E ve Z izomerleriyle olduğu gibi atropizomerleri arasındaki dönüşüm çalışılmıştır. Bu noktada izomer karışımının içeriği belirlenmek istenmiştir. Yoğunluk Fonksiyonu Teorisi (DFT) ile yapılan hesaplamalar, E ve Z isomerlerinin eş zamanlı oluşabileceğini ve aynı ortamda bulunabileceğini göstermiştir. E isomerleri arası dönüşüm düşük aktivasyon enerjileri ile gerçekleşebildiğinden oda sıcaklığında E atropisomerlerinin dönüşümünü gözlemlemek mümkündür. Z isomerleri daha yüksek eşik enerjilerine sahip olmalarına rağmen zaman faktörüne dayalı söz konusu eşikleri aşabilmek mümkündür. İkinci kısımda, 1,2-diazin ve siloksi alkin siklik katılım tepkimelerinde geçiş metali etkisi incelenmiştir. Bir geçiş metali olan gümüş(I) metalinin aktivasyon enerjisini düşürmesi açısından 1,2-diazin ve siloksi alkin siklik katılım tepkimelerinde önemli bir rolü olduğu gösterilmiştir. Bununla beraber, 1,2-diazin ve siloksi alkine sübstitüyent etkisi de incelenmiştir. Relativistik Yoğunluk Fonksiyonu Teorisi (DFT) ile yapılan hesaplamalar, katalizörün orbitaller arası enerji farkını düşürerek dienofilin HOMO ve dienin LUMO etkileşimini kolaylaştırdığını kanıtlamıştır. Katalizörün 1,2-diazin ve siloksi alkin Diels-Alder tepkimelerini normal şartlar altında mümkün kıldığını gösterdikten sonra, muhtemel tepkime mekanizmaları da incelenmiştir.

TABLE OF CONTENTS

LIST OF FIGURES

LIST OF TABLES

LIST OF SYMBOLS

E_c^{VWN}	Vosko-Wilk-Nusair correlation functional
E_x^{exact}	Exact exchange energy
$E_c[\rho]$	Correlation energy
$E_x[\rho]$	Exchange energy
$E_{\sigma\sigma^*}$	Non-covalent contributions to the energy
$G^{\ddagger}$	Gibbs free energy of activation
$J[\rho]$	Coulomb energy
$T[\rho]$	Kinetic energy of interacting electrons
$T_s[\rho]$	Kinetic energy of non-interacting electrons
U_x^{σ}	Exchange energy density
$V_{ee}[\rho(r)]$	Interelectronic interactions
$V_{ext}(r)$	External potential
V_{KS}	Kohn-Sham potential
ΔE_x^{B88}	Becke's gradient correction
ΔE_0	Relative electronic energy at 0 K
ΔH_{rxn}	Heat of reaction
$v(r)$	External potential
$\rho(r)$	Electron density
ψi	Kohn-Sham orbitals

LIST OF ACRONYMS/ABBREVIATIONS

B3LYP	Becke-3-parameter Lee-Yang-Parr functional
B88	Becke 88 Exchange Functional
DFT	Density functional theory
HF	Hartree-Fock theory
LDA	Local density approximation
M062X	Empirical exchange-correlation functionals
M06-L	Empirical local functionals
MPW1K	Modified Perdew-Wang 1 Parameter Method for Kinetic
ωB97XD	Head-Gordon emprical dispersion functionals

1. INTRODUCTION

1.1. Cyanoisoindole Containing Strigolactone Analogues

Strigolactones are a new class of plant derived terpenoids and are isolated from their root exudates. The function of strigolactones in plant biology has been recognized as the signaling molecule inducing one of the most abundant symbiosis processes in nature [1]. Strigolactones have more recently been shown to have much broader communication roles. Besides having host-parasite interactions both in plants and mycorrhizal fungi, strigolactones have also been shown to have hormonal roles in higher plants [2].

At the time of their discovery, research on these small molecule communicators raised some interesting questions as to how these small molecules evolved. Furthermore, their structures are complex rendering their unambiguous determination, isolation and synthesis demanding. However, over the years progress has been made that enables the identification of some structural features of active strigolactones. Strigolactone structures are generally classified as having a tri-cyclic apocarotenoid (A, B or C rings) connected to γ-butyrolactone (D-ring) through an enol ether bond.

Among these four important structural regions, the lactone D-ring is of importance in terms of biological activity. On the other hand, the ester contained within the C ring was found to be unimportant for biological activity. The remaining A and B-rings give a lot of structural freedom; as such there may be enhanced activity in the case of H-bond acceptors present on A and B-rings.

In addition to strigol representative example (Figure 1.1), many other strigolactone analogues are available in plant life such as 1-cyano-isoindoles. This analogue of strigolactones provides more information on its exact location in the plant cell through the introduction of fluorescence. Further on, the isoindole backbone is an efficient marker in biological assays and a wide variety of fluorescent enzyme ligands [3].

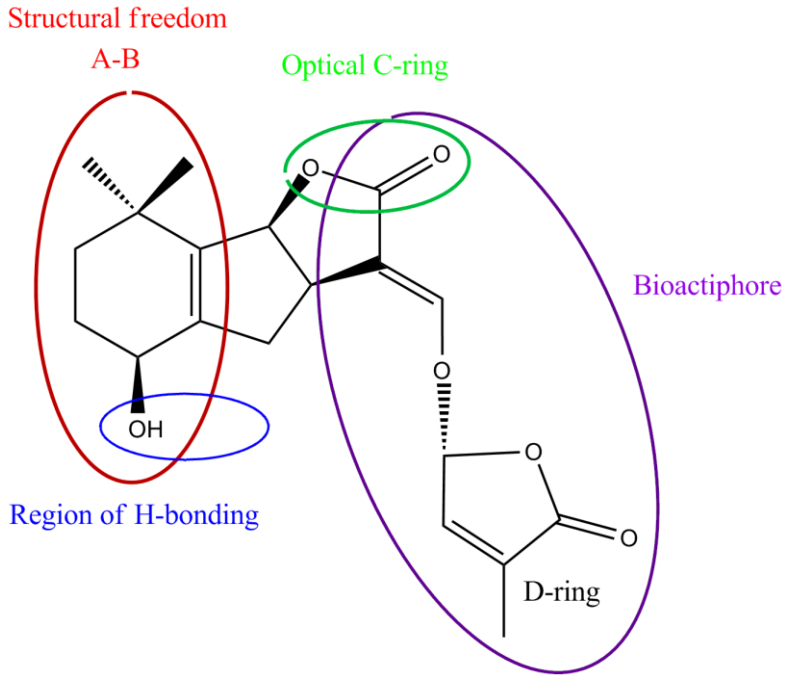

Figure 1.1. (+)-Strigol.

A schematic representation of 1-cyanoisoindole containing strigolactone synthesis is depicted in Figure 1.2. Moving back to strigolactones, introduction of an enol ether linked D-ring is essential, as seen in the case of strigolactone analogue 3 (Figure 1.2), renders it biologically active.

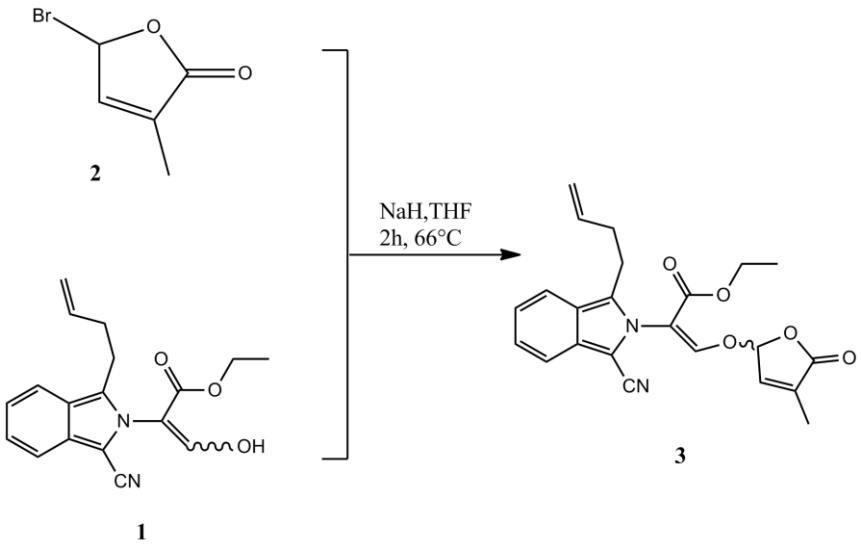

Figure 1.2. Synthesis of strigolactone analogue 3.

1.2. Isomers of Strigolactone Analogues

Strigolactone analogues containing an enol ether linkage can be seen as isomeric mixtures due to the sp^2 hybridization they possess. The stereo center of 1 (Figure 1.2) is subjected to both *Re* and *Si* face attack (Figure 1.3) that finally produce a racemic mixture ensuing, namely, from E/Z isomers of strigolactone 3.

Recently, Rasmussen *et al.* performed experiments concerning the isolation of strigolactone analogues at room temperature [4]. These experimental studies on the detection of strigolactone 3 which was isolated in 81% yield provide some information about its isomeric ratios. NMR analysis exposed that this strigolactone analogue was isolated as a 45:55 mixture of isomers which appears to interconvert at room temperature (Figure 1.4). However, the exact nature of the isomers remains undetermined via experimental analysis techniques.

Chirality plays a crucial role in many biological systems regarding the activity of the target molecule. In the case of strigolactone 3, enantioselective introduction of the D-ring produces two possible enantiomers (R) and (S) on the ring (Figure 1.3). Besides the chirality of the D-ring, there is also an axial chirality concerning the isoindole ring. An enantioselective introduction to an already chiral system yields a mixture of diastereomers as depicted in Figure 1.3 and explained in more detail in Figure 1.6 in the following section.

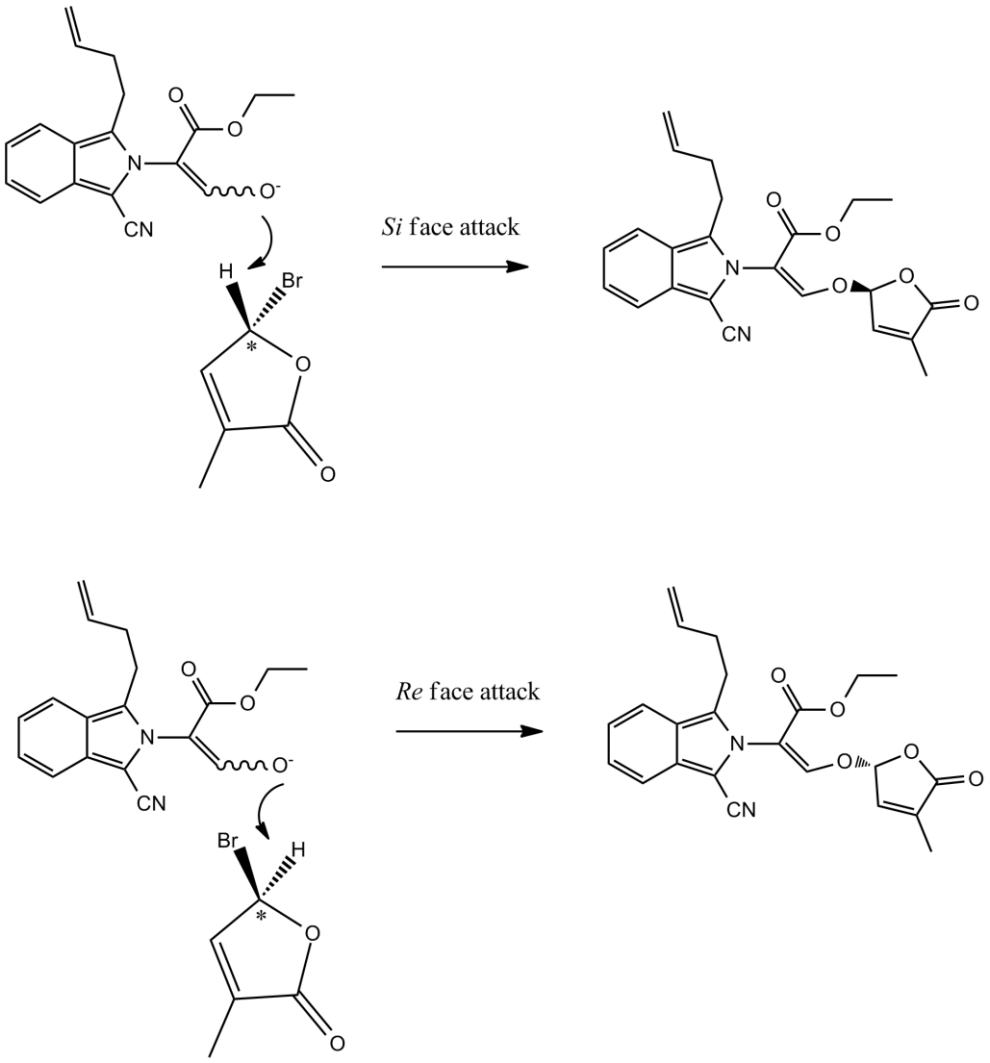

Figure 1.3. Enantioselective formation of strigolactone 3.

1.3. Rotational Isomerization of Strigolactone Analogues

Many molecules can undergo rotational isomerization around one or more of their chemical bonds. On the course of isomerization, a molecule shifts between relatively stable conformations by passing through unstable configurations. Rotational isomerization is a major factor in the dynamics, reactivity and biological activity of molecular structures [5].

The hypothetical reaction in Figure 1.4 takes place through a rotational isomerization mechanism. As a first attempt, E/Z mixture which is our primary effort to distinguish is expected to exist in the reaction medium. However, before the isolation of

two potential isomers a more intriguing question of that by which means, rotation around a restricted double bond can be achieved attracts the attention of both experimental and computational chemists.

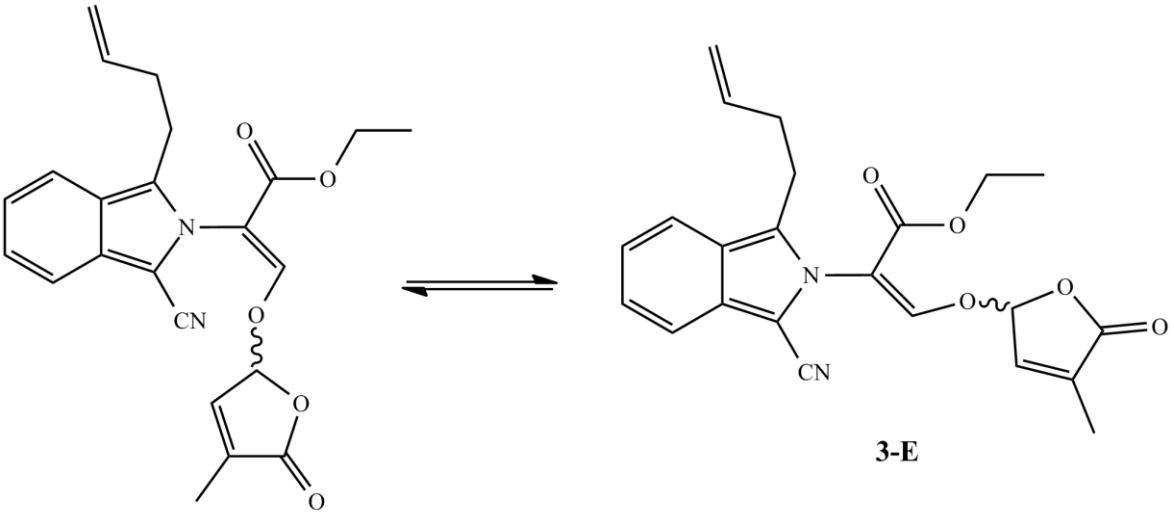

Figure 1.4. A hypothetical interconversion of E and Z isomers.

Considering the conjugated π system present in strigolactone 3, the double bond that connects the enol ether and the isoindole together has a partial double bond character. Thus, electron delocalization from nitrogen lone pairs to sp^2 C=C center allows the rotation around the bond of interest. Consequently, due to the resonance contribution in the molecular system the molecule can inherently be present in two isomeric forms.

That being said, one point to be alert is the plane of the aromatic isoindole ring and that of the enol ether. Conjugation can take place between the two planes so long as the angle between these planes is plausibly small or they are coplanar. If there is no conjugation between these π systems, this offers a completely different possible explanation for the formation of two isomers.

To this end, one attempt can be to break the double bond about the alkene stereo center by the attack of a nucleophile to the molecule. Strigolactone 3 is isolated under basic conditions in the reaction medium. Hence, 1,4-addition of hydroxyl OH^- ion (Figure 1.5) is considered to enable the conversion of sp^2 hybridized reaction center to a sp^3 hybridized single bond around which a rotation is more likely.

A nucleophilic addition to an unsaturated stereo center can occur from both sites so called *Re* and *Si* face and result in two distinctive products. Once the double bond is cleaved by a nucleophilic addition, an E isomer can convert into Z isomer or vice versa under certain conditions.

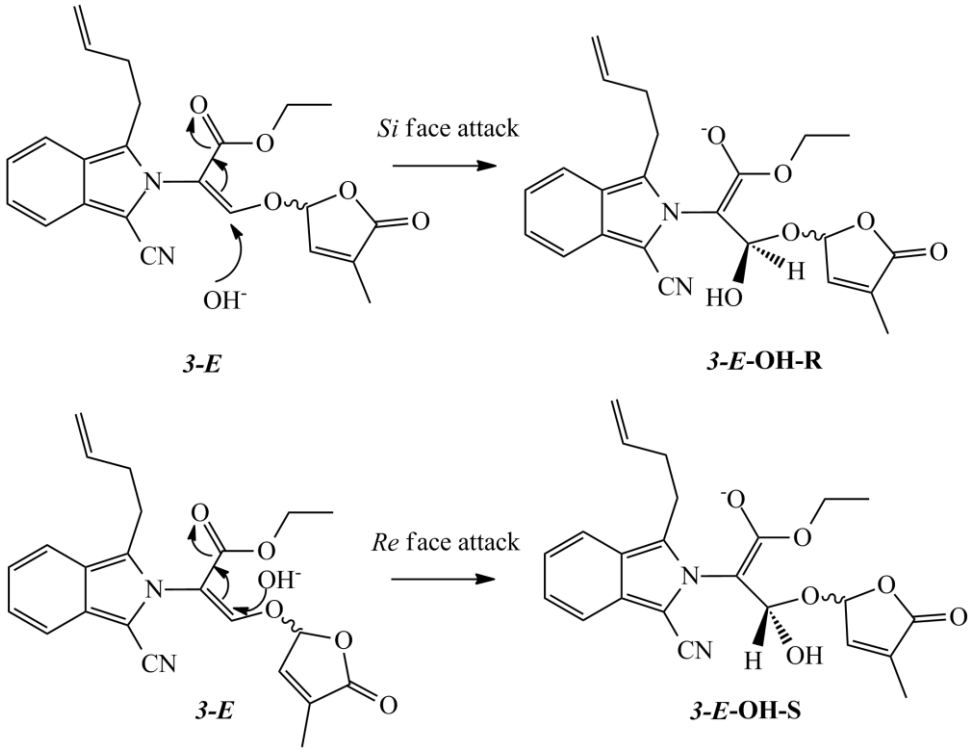

Figure 1.5. Nucleophilic addition of OH^- to the strigolactone 3.

1.3.1. Atropisomerism of Strigolactone Analogue

Restricted rotation around single bonds in molecules can result in the formation of atropisomers [6]. Atropisomers possess high steric strain barriers to rotation that allow the isolation of the conformers [7]. In the case of strigolactone 3, a hindered rotation around the N-C bond is anticipated due to the tilted conformation relative to the molecular plane and hence an axial chirality is delineated. Apart from the rotation about the pro-single bond, a rotation around the N-C bond linking isoindole and enol ether is anticipated. If there is a slow rotation along this bond, two rotational isomers can be observed by NMR and on the NMR-timescale a center of molecular chirality is introduced. As there is a chiral

center included in the D-ring, which was racemically formed, a mixture of diastereomers can be observed (Figure 1.6).

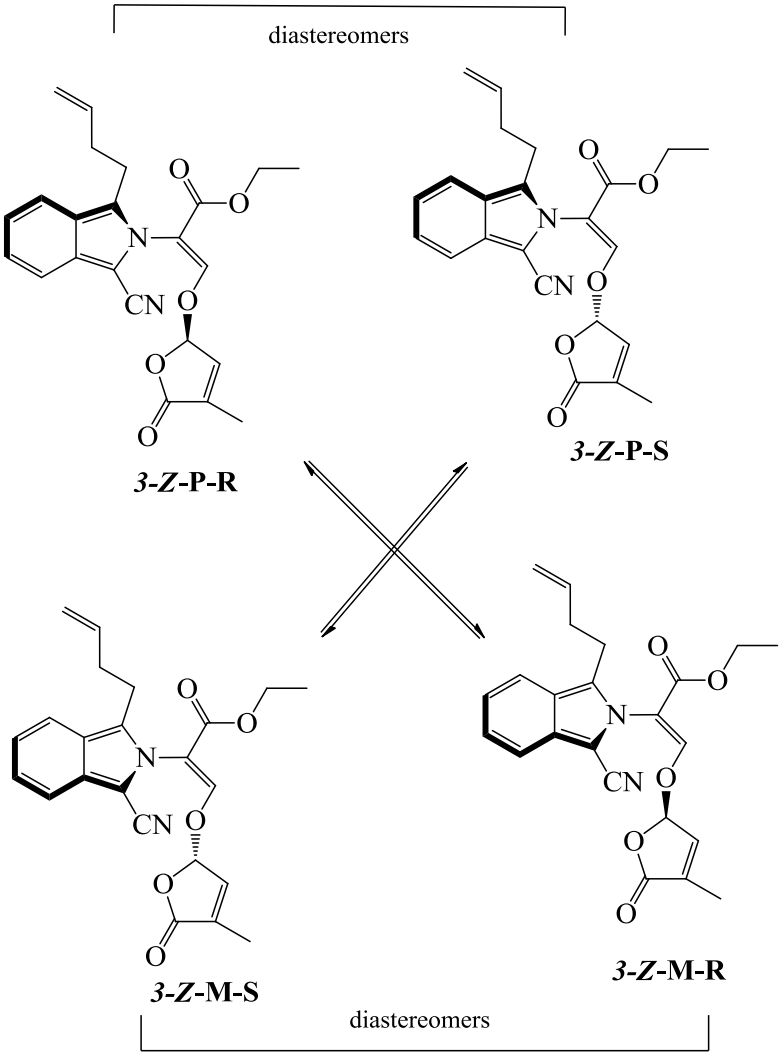

Figure 1.6. Diastereomers and enantiomers of strigolactone 3 for Z isomer.

The aim of this study is to investigate the ratio of E/Z isomers and shed light on the predominance of each one. Rationalization of the surpassing isomer via quantum mechanical methods will provide an understanding of the exact nature of E/Z isomers and permit the experimental chemists to detect and isolate the proposed E/Z mixture for which NMR and other experimental analysis techniques prove insufficient information.

2. METHODOLOGY

2.1. Density Functional Theory

The entire field of density functional theory rests on two fundamental mathematical theorems proved by Kohn and Hohenberg. The first theorem proved by Hohenberg and Kohn is stated as 'The ground state energy from Schrödinger equation is a unique functional of the electron density'. The second theorem defines the important property of this unique functional that the electron density that minimizes the energy of the overall functional is the true electron density yielding the full solution of Schrödinger equation [8]. Kohn-Hohenberg theorems proposed in the mid 1960s [9-10] are the basic idea of the density functional theory (DFT) [11] which is the quantum mechanical approach of the electronic structure of atoms and molecules. The first theorem states that the electron density ρ(r) determines the external potential V_{ext}(r) and the second theorem introduces the variational principle. As a result, the electron density can be computed variationally and the position of nuclei, energy, wave function and other related parameters (i.e. every observable of a stationary quantum mechanical system) can be calculated from the ground state electron density [11-12].

The electron density is defined as:

$$\rho(x) = N \int \cdots \int |\Psi(x_1, x_2, \cdots, x_n)|^2 dx_1 dx_2 \cdots dx_n \tag{2.1}$$

where *x* represents both spin and spatial coordinates of electrons.

The electronic energy can be expressed as a functional of the electron density:

$$E[\rho] = \int v(r)\rho(r)dr + T[\rho] + V_{ee}[\rho] \tag{2.2}$$

where $T[\rho]$ is the kinetic energy of the interacting electrons and $V_{ee}[\rho]$ is the interelectronic interaction energy. The electronic energy may be rewritten as

$$E[\rho] = \int v(r)\rho(r)dr + T_s[\rho] + J[\rho] + E_{xc}[\rho] \tag{2.3}$$

with $J[\rho]$ being the coulomb energy, $T_s[\rho]$ being the kinetic energy of the non-interacting electrons and $E_{xc}[\rho]$ being the exchange-correlation energy functional. The exchange-correlation functional is expressed as the sum of an exchange functional $E_x[\rho]$ and a correlation functional $E_c[\rho]$, although it contains also a kinetic energy term arising from the kinetic energy difference between the interacting and non-interacting electron systems. The Coulomb energy term describes the unfavorable electron-electron repulsion energy and therefore disfavors the total electronic energy [13].

In Kohn-Sham density functional theory, a reference system of independent non-interacting electrons in a common, one-body potential V_{KS} yielding the same density as the real fully-interacting system is considered. More specifically, a set of independent reference orbitals ψ_i satisfying the following independent particle Schrödinger equation is imagined.

$$\left[-\frac{1}{2}\nabla^2 + V_{KS}\right]\psi_i = \varepsilon_i\psi_i \tag{2.4}$$

with the one-body potential V_{KS} defined as

$$V_{KS} = v(r) + \frac{\partial J[\rho]}{\partial\rho(r)} + \frac{\partial E_{xc}[\rho]}{\partial\rho(r)} \tag{2.5}$$

$$V_{KS} = v(r) + \frac{\rho(r')}{|r - r'|}dr' + v_{xc}(r) \tag{2.6}$$

where $v_{xc}(r)$ is the exchange-correlation potential. The independent orbitals ψ_i are known as Kohn-Sham orbitals and give the exact density by

$$\rho(r) = \sum_i^N |\psi_i|^2 \tag{2.7}$$

if the exact form of the exchange-correlation functional is known. However, the exact form of this functional is not known and approximate forms are developed starting with the local density approximation (LDA). This approximation gives the energy of a uniform electron gas, i.e. a large number of electrons uniformly spread out in a cube accompanied with a uniform distribution of the positive charge to make the system neutral. The energy expression is

$$E[\rho] = T_s[\rho] + \int \rho(r) v(r) dr + J[\rho] + E_{xc}[\rho] + E_b \tag{2.8}$$

where E_b is the electrostatic energy of the positive background. Since the positive charge density is the negative of the electron density due to uniform distribution of particles, the energy expression is reduced to

$$E[\rho] = T_s[\rho] + E_{xc}[\rho] \tag{2.9}$$

$$E[\rho] = T_s[\rho] + E_x[\rho] + E_c[\rho] \tag{2.10}$$

The kinetic energy functional can be written as

$$T_s[\rho] = C_F \int \rho(r)^{5/3} dr \tag{2.11}$$

where C_F is a constant equal to 2.8712. The exchange functional is given by

$$E_x[\rho] = -C_x \int \rho(r)^{4/3} dr \tag{2.12}$$

with C_x being a constant equal to 0.7386. The correlation energy, $E_c[\rho]$, for a homogeneous electron gas comes from the parameterization of the results of a set of quantum Monte Carlo calculations.

The LDA method underestimates the exchange energy by about 10 per cent and does not have the correct asymptotic behavior. The exact asymptotic behavior of the exchange energy density of any finite many-electron system is given by

$$\lim_{x\to\infty} U_x^{\sigma} = -\frac{1}{r} \tag{2.13}$$

U_x^{σ} being related to $E_x[\rho]$ by

$$E_x[\rho] = \frac{1}{2}\sum_{\sigma}\int \rho_{\sigma} U_x^{\sigma} dr \tag{2.14}$$

A gradient-corrected functional is proposed by Becke

$$E_x = E_x^{LDA} - \beta\sum_{\sigma}\int \rho_{\sigma}^{4/3} \frac{x_{\sigma}^2}{1+6\beta x_{\sigma}\sinh^{-1} x_{\sigma}} dr \tag{2.15}$$

where σ denotes the electron spin, $x_{\sigma} = \dfrac{|\nabla\rho_{\sigma}|}{\rho_{\sigma}^{4/3}}$ and β is an empirical constant (β=0.0042). This functional is known as Becke88 (B88) functional [9].

$$E_{xc} = \int_0^1 U_{xc}^{\lambda} d\lambda \tag{2.16}$$

where λ is the interelectronic coupling-strength parameter and U_{xc}^{λ} is the potential energy of exchange-correlation at intermediate coupling strength. The adiabatic connection formula can be approximated by

$$E_{xc} = \frac{1}{2}E_x^{exact} + \frac{1}{2}U_{xc}^{LDA} \tag{2.17}$$

since $U_{xc}^{0} = E_{x}^{exact}$, the exact exchange energy of the Slater determinant of the Kohn-Sham orbitals, and $U_{xc}^{1} = U_{xc}^{LDA}$ [8].

The closed shell Lee-Yang-Parr (LYP) correlation functional [14] is given by

$$E_c = -a\int \frac{1}{1+d\rho^{-1/3}} \left\{ \rho + b\rho^{-2/3} \left[C_F \rho^{5/3} - 2t_w + (\frac{1}{9}t_w + \frac{1}{18}\nabla^2\rho) \right] e^{-c\rho^{-1/3}} \right\} dr \quad (2.18)$$

where

$$t_w = \frac{1}{8}\frac{|\nabla\rho(r)|^2}{\rho(r)} - \frac{1}{8}\nabla^2\rho \quad (2.19)$$

The mixing of LDA, B88, E_x^{exact} and the gradient-corrected correlation functionals to give the hybrid functionals [15] involves three parameters.

$$E_{xc} = E_{xc}^{LDA} + a_0\left(E_x^{exact} - E_x^{LDA}\right) + a_x\Delta E_x^{B88} + a_c\Delta E_c^{non-local} \quad (2.20)$$

where ΔE_x^{B88} is the Becke's gradient correction to the exchange functional. In the B3LYP functional, the gradient-correction ($\Delta E_c^{non-local}$) to the correlation functional is included in LYP. However, LYP contains also a local correlation term which must be subtracted to yield the correction term only.

$$\Delta E_c^{non-local} = E_c^{LYP} - E_c^{VWN} \quad (2.21)$$

where E_c^{VWN} is the Vosko-Wilk-Nusair correlation functional, a parameterized form of the LDA correlation energy based on Monte Carlo calculations. The empirical coefficients are a_0=0.20, a_x=0.72 and a_c=0.81 [16].

2.2. Continuum Solvation Models

Continuum solvation models are the most efficient way to include condensed-phase effects into quantum mechanical calculations [17]. Advantage of these models is that they decrease the number of the degrees of freedom of the system by describing them in a continuous way, usually by means of a distribution function [18-19]. In continuum solvation models, the solvent is represented as a polarizable medium characterized by its static dielectric constant ε and the solute is embedded in a cavity surrounded by this dielectric medium. The total solvation free energy is defined as

$$\Delta G_{solvation} = \Delta G_{cavity} + \Delta G_{dispersion} + \Delta G_{electrostatic} + \Delta G_{repulsion} \quad (2.22)$$

where ΔG_{cavity} is the energetic cost of placing the solute in the medium. Dispersion interactions between solvent and solute are expressed as $\Delta G_{dispersion}$ which add stabilization to solvation free energy. $\Delta G_{electrostatic}$ is the electrostatic component of the solute-solvent interaction energy. $\Delta G_{repulsion}$ is the exchange solute-solvent interactons not included in the cavitation energy.

The central problem of continuum solvent models is the electrostatic problem described by the general Poisson equation:

$$-\vec{\nabla}\left[\varepsilon(\vec{r})\nabla\vec{V}(\vec{r})\right] = 4\pi\rho_M(\vec{r})$$

simplified to

$$-\nabla^2 V(\vec{r}) = 4\pi\rho_M(\vec{r}) \text{ within } C \quad (2.23)$$

$$-\varepsilon\nabla^2 V(\vec{r}) = 0 \text{ outside } C \quad (2.24)$$

where C is the portion of space occupied by cavity, ε is dielectric function, V is the sum of electrostatic potential V_M generated by the charge distribution ρ_M and the reaction potential V_R generated by the polarization of the dielectric medium:

$$V(\vec{r}) = V_M(\vec{r}) + V_R(\vec{r}) \tag{2.25}$$

Polarizable Continuum Model (PCM) belongs to the class of polarizable continuum solvation models [20]. In PCM, the solute is embedded in a cavity defined by a set of spheres centered on atoms (sometimes only on heavy atoms), having radii defined by the van der Waals radii of the atoms multiplied by a predefined factor (usually 1.2). The cavity surface is then subdivided into small domains (called tesserae), where the polarization charges are placed. There are three different approaches to carry out PCM calculations. The original method is called Dielectric PCM (D-PCM), the second model is the Conductor-like PCM (C-PCM) [21] in which the surrounding medium is modeled as a conductor instead of a dielectric, and the third one is an implementation whereby the PCM equations are recast in an integral equation formalism (IEF-PCM).

2.3. Computational Details

Density functional theory (DFT) was exploited within the Gaussian09 program package [22] throughout the study. All stationary points were fully optimized at the B3LYP level of density functional theory employing the basis set 6-31+G(d) for all atoms in the gas phase and solvent. A systematic conformational analysis considering all rotatable bonds was performed with 3-fold rotation at the B3LYP/6-31+G(d) level. Furthermore, geometry optimizations for energy refinement were carried out both at the B3LYP/6-31+G(d) and M06-2X level of theory within a basis set 6-31+G(d,p) in polarizable continuum model (PCM).

Geometry optimizations alone cannot determine the nature of the stationary points that they attain. In order to characterize a stationary point, either a minima or maxima (saddle point), it is necessary to perform a frequency calculation on the optimized geometry. Transition states correspond to saddle points on the potential energy surface. Thereby, a transition state search attempts to locate stationary points with a single imaginary (negative) frequency [23]. Also, thermal and entropic contributions to the Gibbs free energies are obtained from these frequency calculations.

So as to identify the shape of the potential energy surface, intrinsic reaction coordinate (IRC) calculations were utilized through the transition state structures connecting the reactants and products of the trajectory.

B3LYP is known to yield rather good geometries and ground state properties but usually underestimates activation barriers and weak interaction energies [24]. To the extent DFT shows systematic weaknesses in long range interactions related to nonbonding atoms, parameterized functionals which account for dispersion are resorted. To this end, a dispersion corrected functional M06-2X was employed to take the long range interactions into consideration on the basis of activation energy calculations. As a result, M06-2X and B3LYP thermal contributions were taken into account separately. Likewise, the same protocol was followed for the solvent energies, albeit solvent optimizations were performed in tetrahydrofuran or water. Moving from 6-31+G(d) to 6-31+G(d,p) basis set, an additional p polarization function on H atom was introduced so as to provide sufficient mathematical flexibility to adequately describe the wave function for the given geometry.

Solvent effects were evaluated by using the Polarizable Continuum Model (PCM) using the integral equation formalism variant (IEFPCM) with the radii UFF (default) cavity model. The isolated reactants and transition state structures were envisioned in tetrahydrofuran (ε=7.4257) to be consistent with the experimental conditions.

The population of the isomers both in gas phase and solvent was analyzed by Boltzmann weighted product populations at room temperature. In Boltzmann distribution equation:

$$\frac{n_P}{n_M} = e^{-\frac{\Delta\Delta G}{RT}} \tag{2.26}$$

ΔΔG is the energy difference between the atropisomers in terms of Gibbs free energies, R is the gas constant and T is the temperature. P and M represent the atropisomers of E and Z structures.

Transition state calculations for the interconversion of P and M isomers were performed at 298.15 K regarding the room temperature conditions. The conventional transition state theory was used to obtain the transition state structures within a single negative frequency and activation Gibbs free energies were described as the difference between the activated complex and the reactants. The rate constant k of a unimolecular reaction is expressed [25] in terms of the molecular Gibbs free energy difference between the activated complex and the reactants (with inclusion of zero point vibrational energies):

$$k = \kappa \frac{kT}{h} e^{-\Delta G^{\ddagger}/RT} \tag{2.27}$$

where κ is the transmission coefficient which is assumed to be about 1 [26].

3. RESULTS AND DISCUSSION

3.1. Energetic Considerations of E and Z Isomers

In molecular systems of high degrees of freedom and so less bond torsion, one needs to consider all rotatable bonds for a systematic and extensive conformation search in order to attain energetically favorable molecular structure. Considering strigolactone 3 derivatives (Figure 1.6) we classified all possible stereoisomers as E and Z isomers as well as their atropisomeric mixture (Figure 3.1). Thus, for strigolactone derivatives in this study, we accounted for the degrees of freedom of these biologically important molecules by means of a systematic 3-fold rotation around all rotatable bonds.

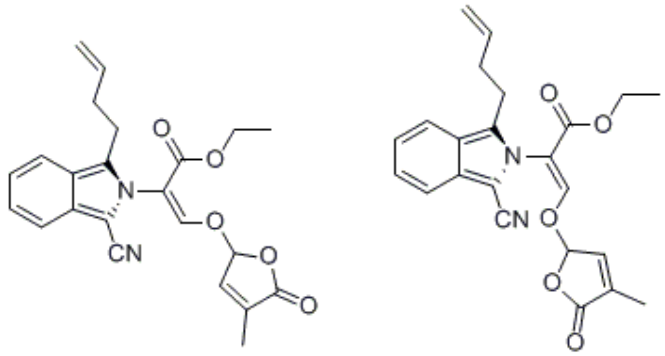

***3-E*-P** ***3-Z*-P**

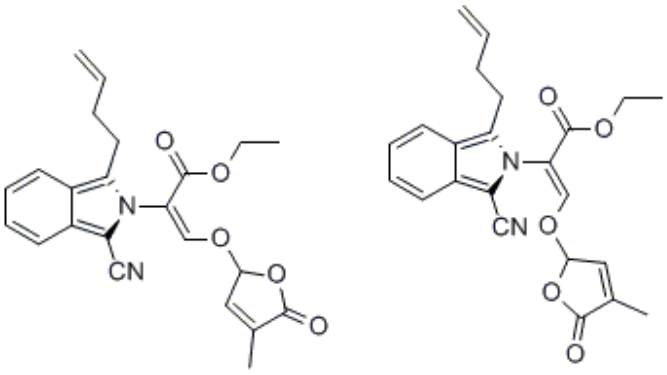

***3-E*-M** ***3-Z*-M**

Figure 3.1. Overview of the possible isomers of the strigolactone 3.

We began with the investigation of the conformational analysis for four different isomers (Figure 3.1). In construing the conformations of E and Z isomers including the P and M structures, R and S configurations of the lactone (D-ring) were also taken into account on the light of possible diastereomers in Figure 1.6. Relative energies of all searched conformers are displayed in Table 3.1. We named the atropisomers as P and M relative to the orientation of the isoindole ring. The more stable *3*-*E*-P isomer was in R configuration, so namely *3*-*E*-P-R while in the case of *3*-*E*-M, S configuration was energetically preferential corresponding to *3*-*E*-M-S. From the viewpoint of Z isomers, the energetically favorable configurations are *3*-*Z*-P and *3*-*Z*-M corresponding to *3*-*Z*-P-S and *3*-*Z*-M-R in relation to S and R configurations respectively.

Table 3.1. Relative Gibbs free energies (kcal/mol) of the most stable isomers of the strigolactone 3.

	3-*E*-P-R	*3*-*E*-M-S	*3*-*Z*-P-S	*3*-*Z*-M-R
B3LYP/6-31+G(d)	3.95	3.79	0.00	0.29
B3LYP/6-31+G(d)[a]	3.08	3.56	0.00	1.39
M06-2X/6-31+G(d,p)[a]	2.48	2.96	0.26	0.0

[a] Polarizable Continuum Model solvent corrections in THF.

3.1.1. Conformational Analysis of E and Z Isomers

Among four isomers, *3*-*Z*-P-S and *3*-*Z*-M-R have the lowest relative Gibbs free energies in comparison with *3*-*E*-P-R and *3*-*E*-M-S isomers. In all these structures, it is obvious that ethyl ester group in the whole strigolactone system is planar, and preferring Z conformation in itself (Figure 3.2). This preference can be attributed to the stabilization effect ensuing from π-π overlap between oxygen p orbital and C=O p-π bond. Destabilization due to the sterically unfavorable ethyl-lactone interactions is avoided by this planarity (Figure 3.3). Additional stabilization is maintained by the in-plane n-orbital on the oxygen atom with the antibonding orbital of the C-O bond (π*).

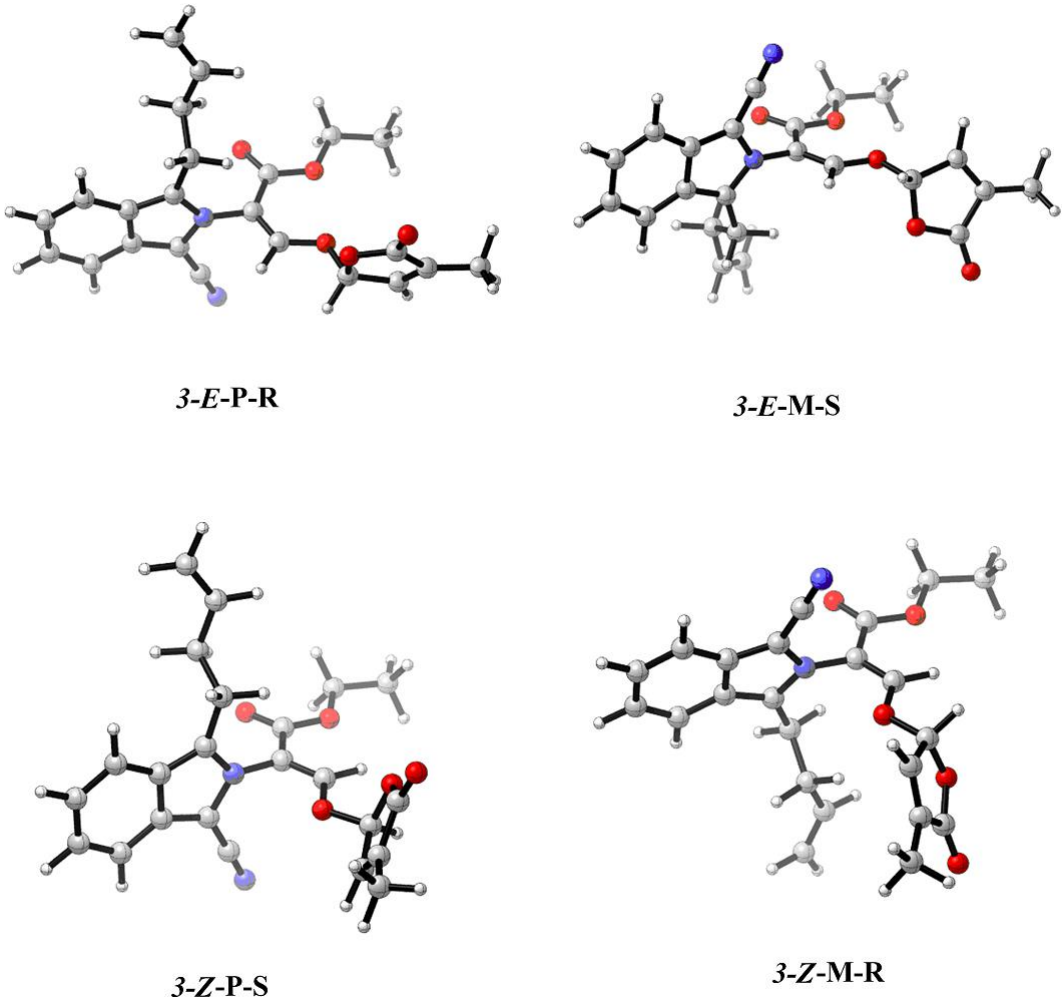

Figure 3.2. Optimized E and Z structures (B3LYP/6-31+G(d) in THF).

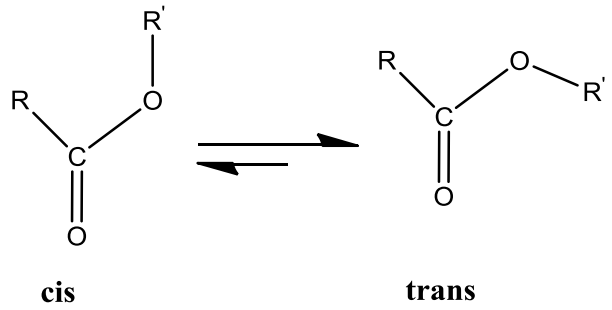

R': CH_2CH_3

R: ∿CN=CHO∿

Figure 3.3. Overview of the ethyl ester conformations in strigolactone 3.

Going back to the E and Z isomers, a plausible reason for the Z conformation preference can be the bifurcated model specific to this case. Alkene hydrogen is stabilized under the influence of ethyl ester and lactone oxygen through weak H-bonding. In the case of *3-Z*-P-S isomer, H-bond distances are 2.38 and 2.71 Å respectively while they are 2.38 and 2.20 for *3-Z*-M-R (Figure 3.4). We observe a smaller difference in THF relative energies of E and Z isomers (Table 3.1) at the M06-2X/6-31+G(d,p) level of theory as this functional accounts more accurately for long range noncovalent interactions such as H-bonding in our situation. Consequently, the more the stabilization factor is included in one of the isomers, the more it transcends over the other.

The stronger H-bonding fashion in *3-Z*-M-R isomer corresponding to 2.41 and 2.80 Å bond lengths in Figure 3.5 renders the M conformation more stable than the P conformation in THF. On the other hand, B3LYP gas phase and condensed phase results demonstrate a different fashion than those of M06-2X with a transcending *3-Z*-P-S though the *3-Z*-M-R has stronger H-bonding interactions. This may stem from the shortcomings of B3LYP to account for weak noncovalent interactions. As a result of increasing the dielectric constant of the medium, which essentially refers to the Polarizable Continuum Model, at M06-2X level of theory, distribution trend in terms of energy shifts towards the more stable *3-Z*-M-R isomer (Table 3.1). Herein, solvation of the molecule acts as an effective contribution as well as weak H-bonding interactions and modeling a system composed of many H-acceptors in a solvent gives a more reliable picture upon the energetics. Overall, it can be deduced that Z isomers may predominate the E isomers in the case of an interconversion.

Proved that M06-2X optimizations do not impact the structures and energetics considerably, we continued with the comparably inexpensive B3LYP/6-31+G(d) level of theory for further calculations throughout the study.

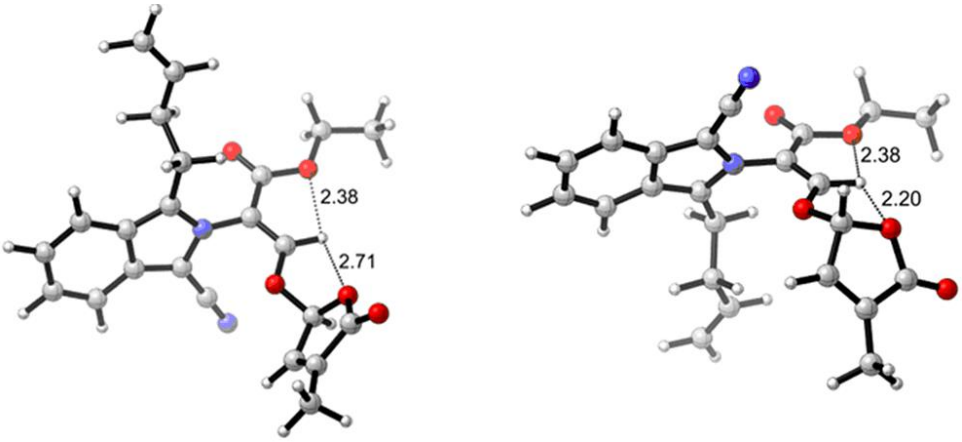

Figure 3.4. H-bonding depiction in Z isomers. Geometry optimizations (B3LYP/6-31+G(d)).

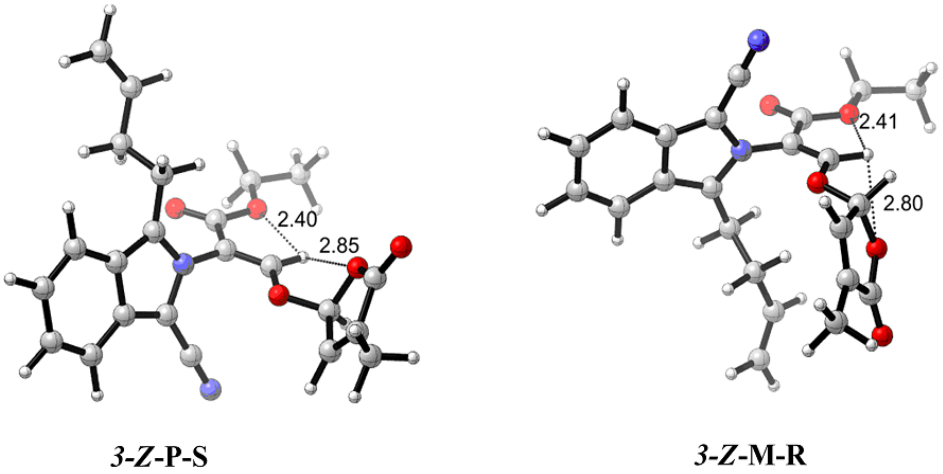

Figure 3.5. H-bonding depiction in Z isomers. Geometry optimizations (M06-2X/6-31+G(d,p) in THF).

Table 3.2. Boltzmann distribution ratios of the possible isomers of the strigolactone 3 (B3LYP/6-31+G(d)).

3-E-P-R/ *3-E*-M-R	*3-E*-P-S/ *3-E*-M-S	*3-Z*-P-R/ *3-Z*-M-R	*3-Z*-P-S/ *3-Z*-M-S
88/12	8/92	5/95	86/14

From the Boltzmann distribution ratios in Table 3.2, both P and M rotamers for E and Z can be observed in the same medium despite a fluctuating population distribution. Even though, Z isomers constitute the preferential structure of the strigolactone 3 as a result of more stable nature over E isomers in accordance with the data in Table 3.1, *3-E*-P and *3-Z*-P isomers as well as the M conformers may be observed together. So as to interpret the population distributions of E and Z isomers and to determine the predominant species we need more lucid expositions. Therefore, we further carried on the formation mechanism of the strigolactone 3 isomers.

3.2. Formation of E and Z Isomers

Thus far, we concluded that Z isomers are energetically more stable than the E isomers and Boltzmann population ratios confirmed that E and Z isomers can exist simultaneously with their P and M rotamers; stable atropisomers appear to coexist. On the light of these findings, we continued with the formations of E and Z isomers separately. In doing so, we aimed to address the feasibility of the formation reactions on the basis of reaction dynamics. The formation of E and Z isomers (3) from bromolactone (2) and deprotonated isoindole (4) is depicted in Figure 3.6. The four possible strigolactone 3 compounds were envisioned and hence their production mechanisms were also studied.

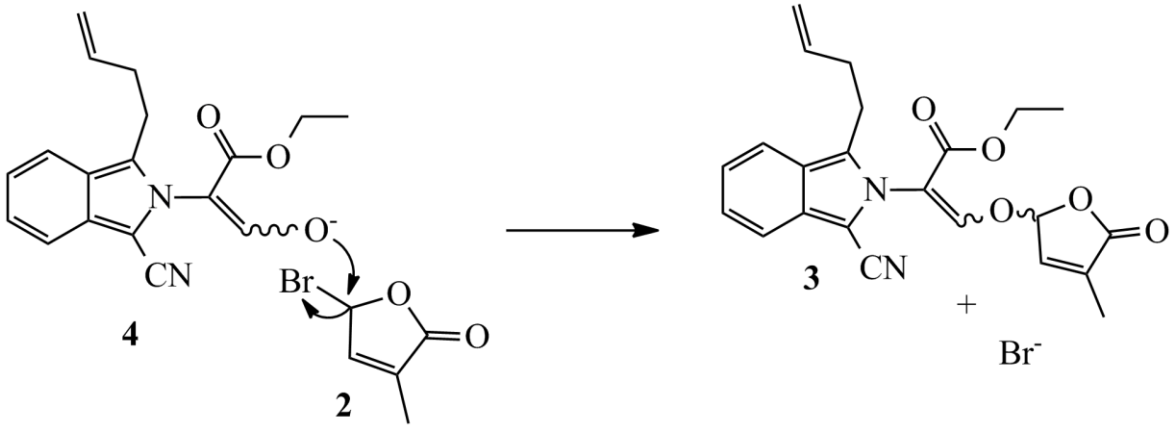

Figure 3.6. Formation of the E and Z isomers through an S_N2 mechanism.

As seen from Table 3.3, E and Z isomers are formed readily at room temperature. In the framework of activation energies of these two isomers, Z transition structures

slightly outweigh over E transition structures. IRC calculations offer *3-E*-P-R and *3-E*-M-S products while in the case of Z isomer *3-Z*-P-S and *3-Z*-M-R were seen. As for the *3-Z*-P-S and *3-Z*-M-R conformers of the predominant Z isomer (Table 3.1), the former was more apparent in general. Moreover, reactants of Z isomer confirm the predominance of *4-Z*-P_R over *4-Z*-M_R (Table 3.3). However, this slight difference proves both species, namely P and M atropisomers, can exist concurrently.

Table 3.3. Gibbs free energies of activation, relative energies of reactants (kcal/mol) for the formation of E and Z isomers and their Boltzmann distribution ratios.

	3-E-P-TS	*3-E*-M-TS	*3-Z*-P-TS	*3-Z*-M-TS
B3LYP/6-31+G(d)	11.7	11.7	11.0	11.0
B3LYP/6-31+G(d)[a]	16.8	16.6	17.0	16.6
	4-E-P_R	*4-E*-M_R	*4-Z*-P_R	*4-Z*-M_R
B3LYP/6-31+G(d)	4.2	4.2	0.0	0.1
B3LYP/6-31+G(d)[a]	3.5	3.5	0.0	0.3
	4-E-P_R/*4-E*-M_R		*4-Z*-P_R/*4-Z*-M_R	
B3LYP/6-31+G(d)	50/50		55/45	
B3LYP/6-31+G(d)[a]	50/50		61/39	

[a] Polarizable Continuum Model solvent corrections in THF.

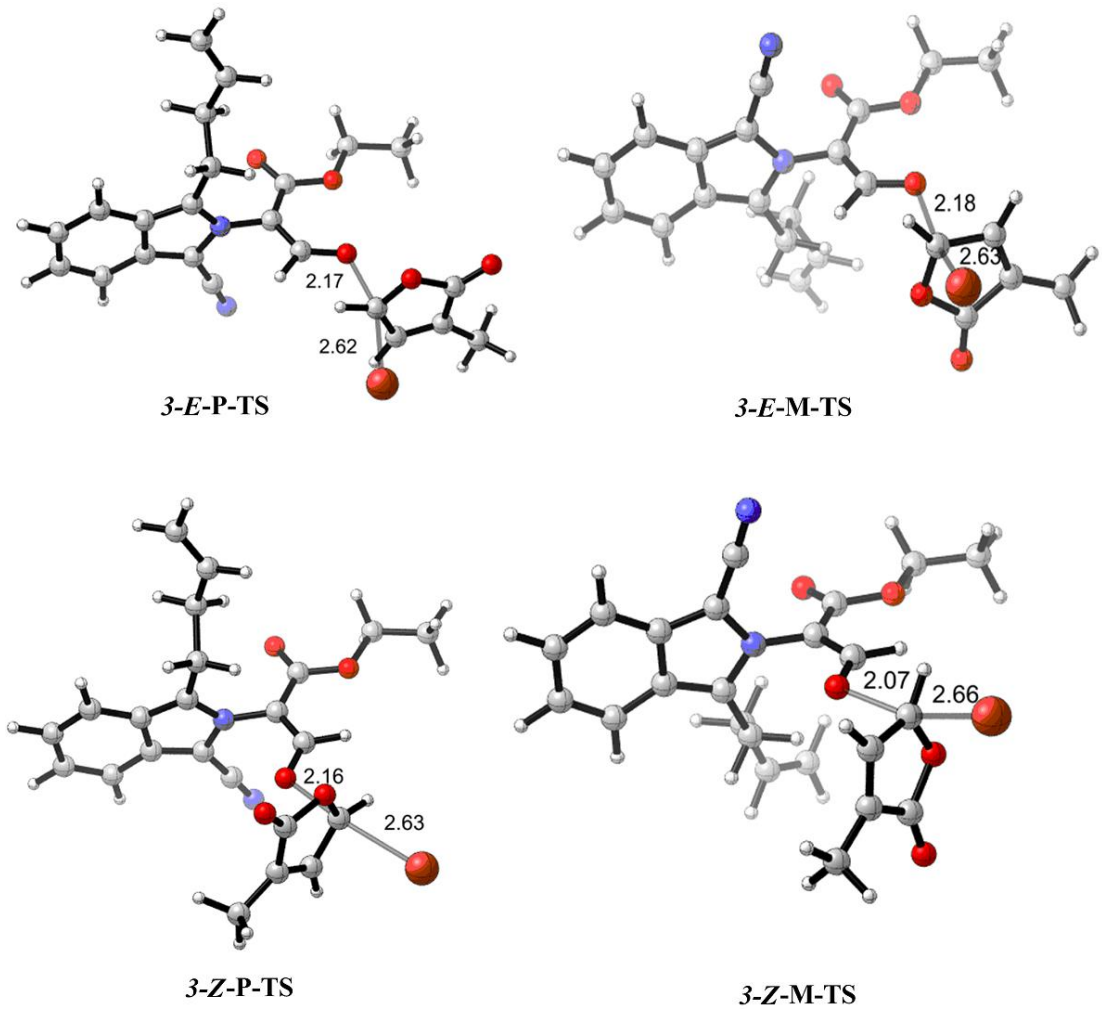

Figure 3.7. Transition state structures for the formation of E and Z isomers (B3LYP/6-31+G(d) in THF).

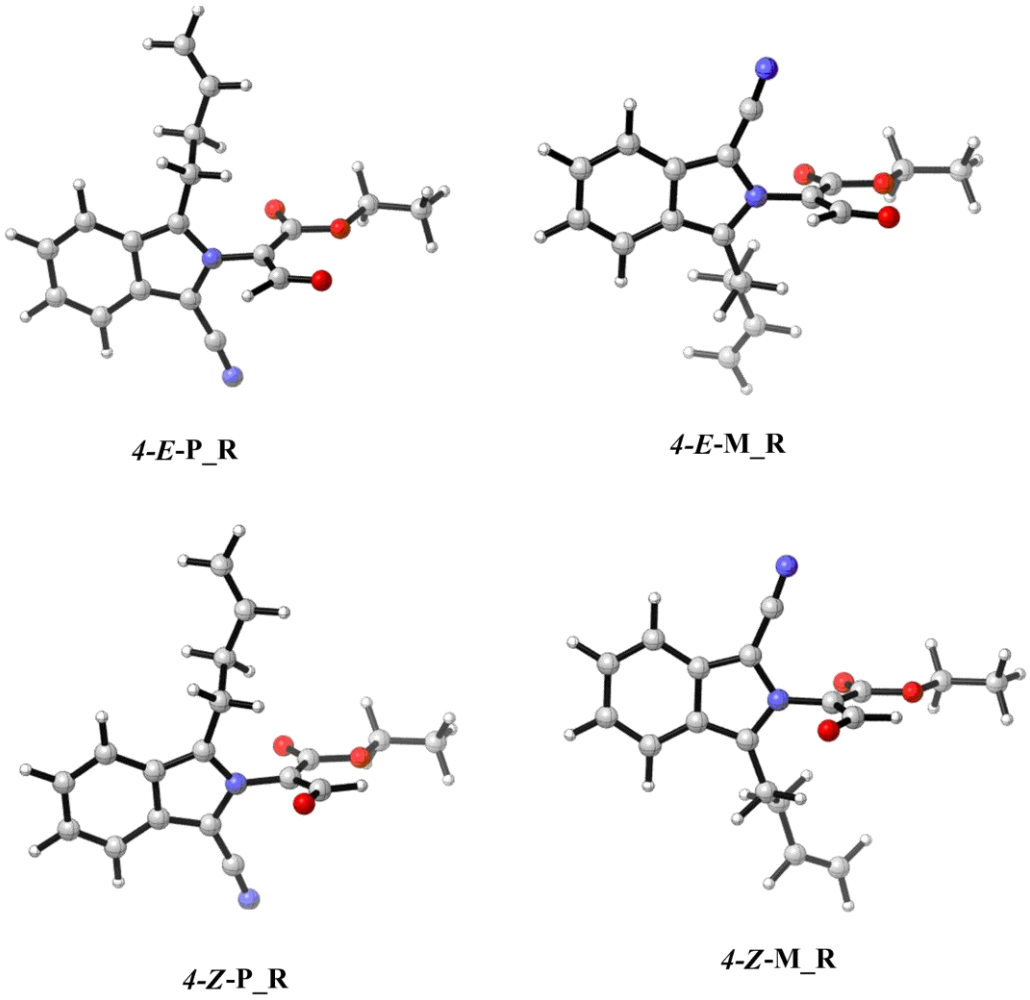

Figure 3.8. Reactants for the formation of E and Z isomers (B3LYP/6-31+G(d) in THF).

3.3. Interconversion of E and Z Isomers

Moving back to our primary goal of determining the nature of the isomeric mixture, we examined the interconversion of E and Z isomers. To this end, as a first attempt we considered the resonance contribution of the cyanoisoindole through the enol ether in the strigolactone 3. In effect, we anticipated a partial double bond character on the isoindole nitrogen and a following enolate formation that can permit a free rotation about the alkene stereo center.

The representative potential energy surface (PES in Figure 3.9) is obtained from a maxima around 140° dihedral. The nuclear geometry of this structure on the PES corresponds to the transition structure of *3-E*-P-R→*3-Z*-P-R for a rotational mechanism.

Optimized geometries of this transition state (*TS*-rot) and corresponding reactant prove that the highlighted resonance effect does not provide a mechanistic ease as the barrier height for this transition is 51.7 kcal/mol (in terms of activation Gibbs free energy). When considering the activation energy required for the rotation around the alkene center, it appears unlikely at room temperature. This can be attributed to the dihedral angle ϕ=122.9° (*TS*-rot a-b-c-d) between isoindole ring and alkene carbon which is far away from planarity.

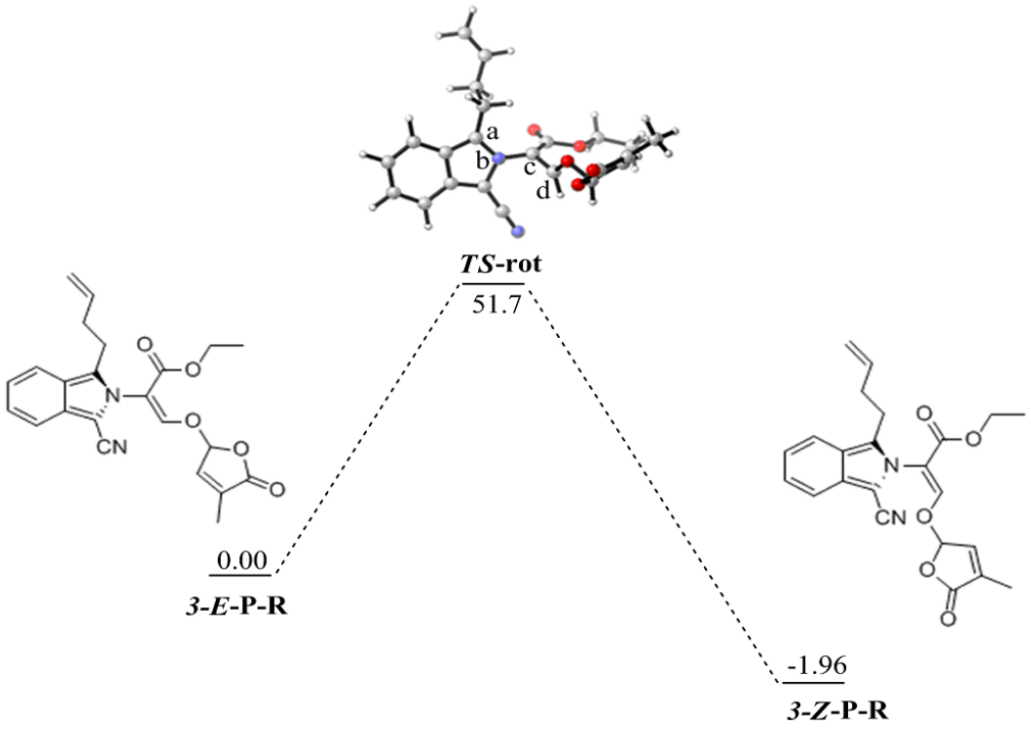

Figure 3.9. Relative Gibbs free energy profile for *3-E*-P-R→*3-Z*-P-R interconversion (B3LYP/6-31+G(d)).

In an effort to warrant a rotation at the alkene center, we attempted to introduce hydroxyl ion as a nucleophile. As a result of cleaving the alkene double bond, we ensured the rotation of *3-E*-P-R into *3-Z*-P-R (Figure 3.10). The presented energy profile was also considered in PCM as well as in the gas phase.

Relative Gibbs free energies in Figure 3.10 expose rather stable intermediates so that a forward reaction to *3-Z*-P-R formation seems very difficult. Once intermediate-2 is

formed, for a transition through the step 3 corresponding to hydroxyl release quite a great barrier height has to be overcome, 17.2 and 21.3 kcal/mol in solvent and vacuum respectively. On the other hand, reverse activation energies for the same intermediate are 7.4 and 4.4 kcal/mol for both cases respectively. This prompts us to expect equilibrium established in the backward direction. Seemingly, formation of *3-Z*-P-R isomer from *3-E*-P-R upon nucleophilic addition of hydroxyl does not provide a conclusive explanation for the interconversion.

OH^- addition protocol was also followed by a Si face attack to the alkene center and the corresponding energy profile was depicted in Figure 3.11. Likewise the Re face attack, too stable intermediate formations were viewed.

Si and Re face attack reaction pathways verified our previous findings that a conversion from *3-E*-P-R to *3-Z*-P-R is unlikely, whence there is even no trace of E alongside the Z isomer.

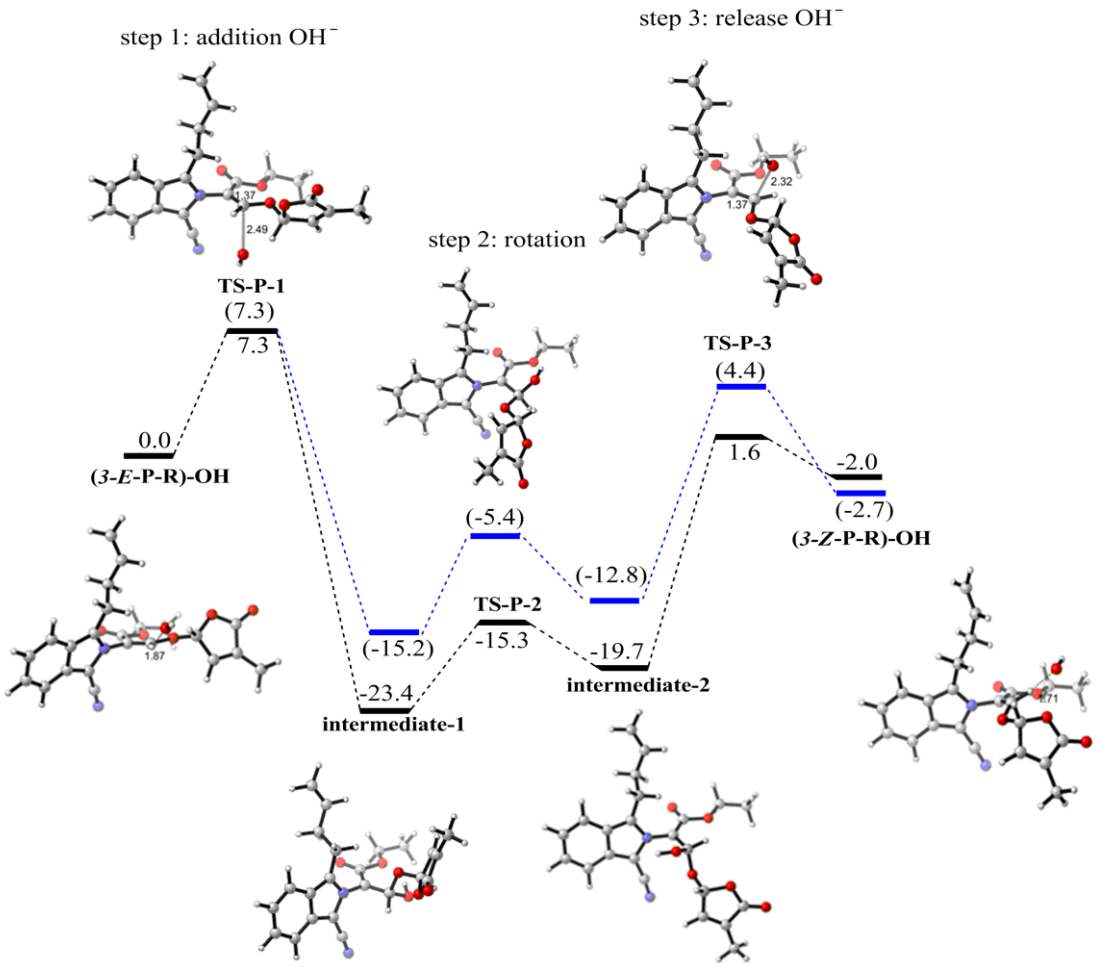

Figure 3.10. Relative Gibbs free energy profile (kcal/mol) for the conversion of *3-E*-P-R to *3-Z*-P-R with OH^- for the Re face attack (B3LYP/6-31+G(d)). PCM optimization results are presented in parenthesis.

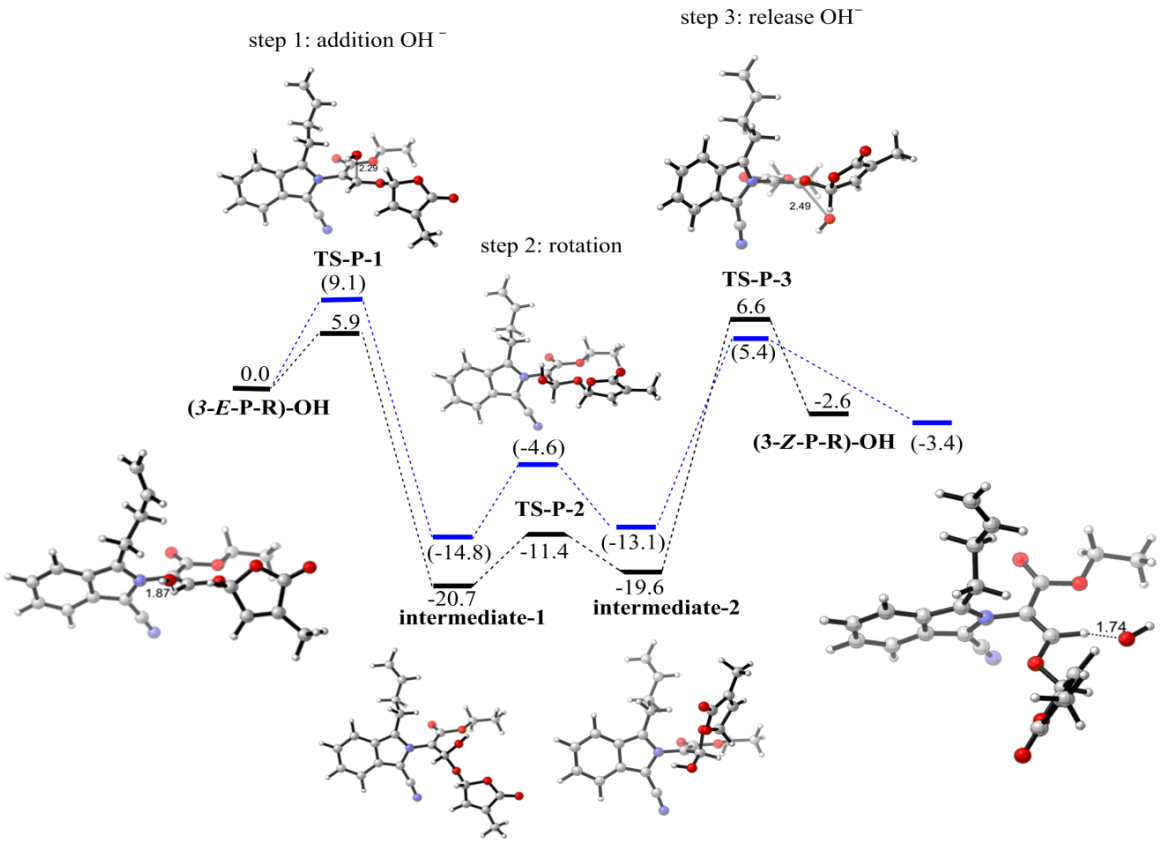

Figure 3.11. Relative Gibbs free energy profile (kcal/mol) for the conversion of *3-E*-P-R to *3-Z*-P-R with OH^- for the Si face attack (B3LYP/6-31+G(d)). PCM optimization results are presented in parenthesis.

3.4. Interconversion of Atropisomers

Ongoing from formation reactions of the strigolactone 3 both in E and Z isomers as well as P and M conformers, our next attempt has been to investigate the interconversion through the hindered rotation around the isoindole-ethyl ester linkage. Rotational mechanism around the single bond of interest suggests two distinctive transition structures because of the rotation in two different ways. The clockwise rotation of the isoindole ring in E isomers around the N-C single bond, which is a linkage through the ethyl ester, resulted in *TS-E-rot* (Figure 3.12). On the other hand, a counter clockwise rotation generated *TS-E'-rot* (Figure 3.12).

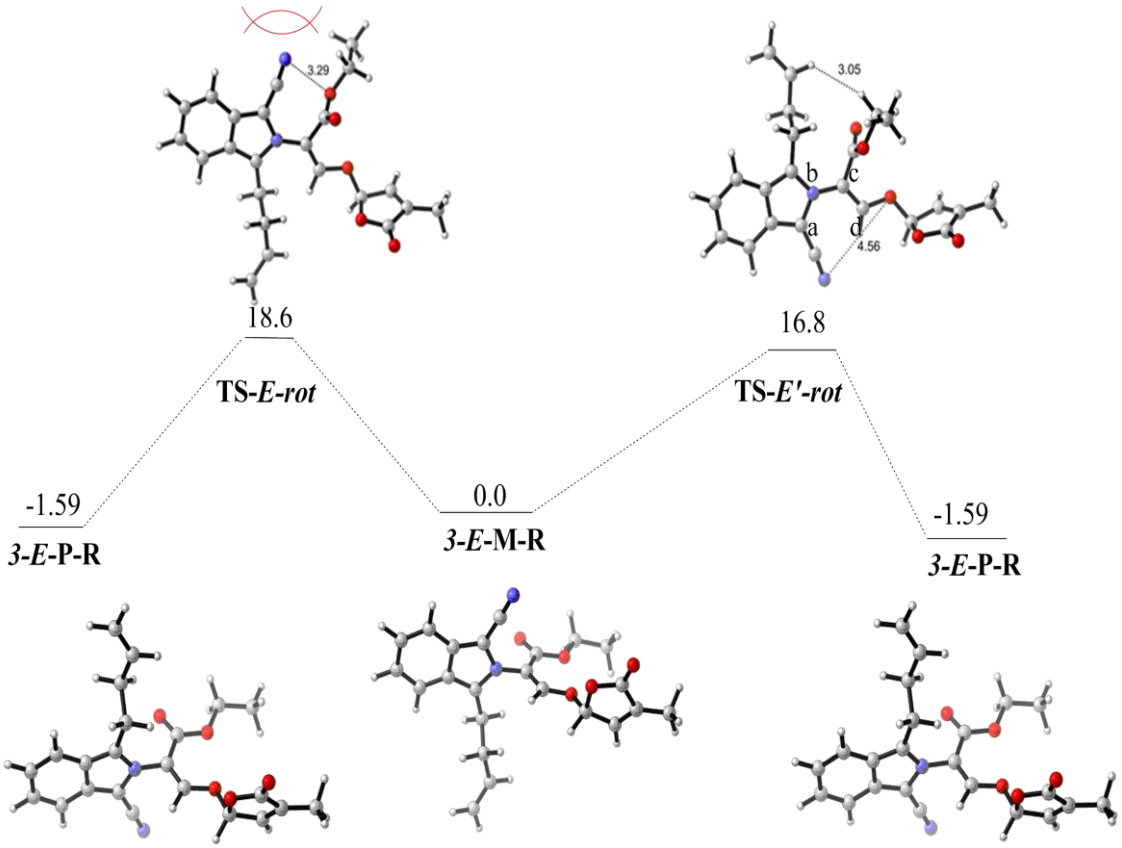

Figure 3.12. Interconversion of *3-E*-P-R and *3-E*-M-R isomer (B3LYP/6-31+G(d) in THF). Relative Gibbs free energies are in kcal/mol.

Giving the activation energies of barrier for the E isomer (Figure 3.12), the energetics of two transitions differ based on the unfavorable O-N interactions in TS-*E-rot*. As the forward barrier heights around 17-19 kcal/mol (Table 3.4) are associated with very rapid reaction times obtained from the Eyring equation (less than 1000 sec), separation of *3-E*-P and *3-E*-M is not possible at room temperature.

Likewise, two different transition structures for the Z isomer (Figure 3.13) were considered and a very slight difference in energetics was encountered. On the other hand, the $\Delta G^{\pm}$ is far higher for the Z case (Table 3.4), in both forward and reverse directions, in comparison to E, drawing attention to the lactone sides of the rotating isoindole that are hindered. Moreover, the repulsive Coulombic interactions of the electronegative oxygen and nitrogen atoms in proximity (Figure 3.13) are also worth stating. Upon time factor and

thermodynamic control, these high barriers can be overcome resulting in an equilibrium and two stable atropisomers of Z can coexist at room temperature.

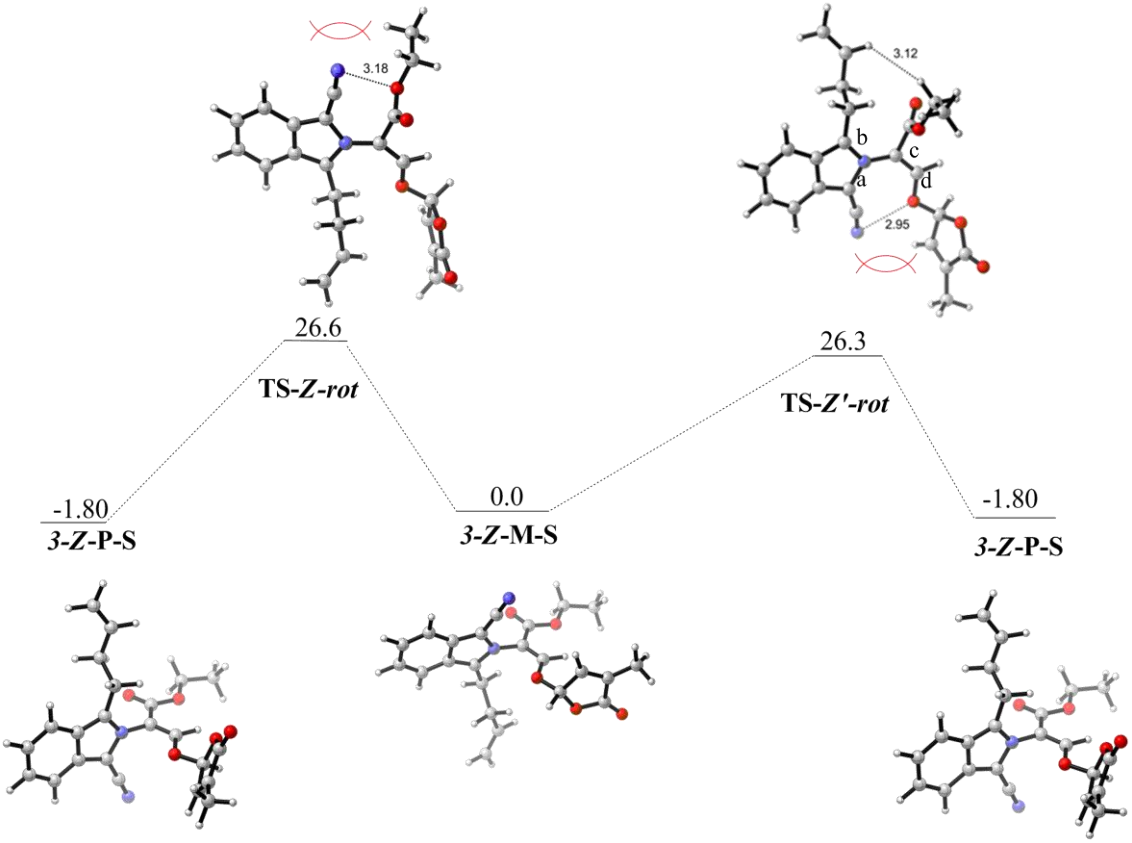

Figure 3.13. Interconversion of *3-Z*-P-S and *3-Z*-M-S isomers (B3LYP/6-31+G(d) in THF). Relative Gibbs free energies are in kcal/mol.

Table 3.4. Gibbs free energy of activation (kcal/mol) for the interconversion of M→P. Reverse activation free energies (P→M) are presented in parenthesis.

	TS-*E-rot*	TS-*E'-rot*	TS-*Z-rot*	TS-*Z'-rot*
B3LYP/6-31+G(d)	17.0 (18.2)	14.5 (15.7)	26.2 (27.3)	24.4 (25.5)
B3LYP/6-31+G(d)[a]	18.6 (20.2)	16.8 (18.4)	26.6 (28.4)	26.3 (28.1)

[a] Polarizable Continuum Model solvent corrections in THF.

The differences in transition structures and ground state structures for both E and Z within the framework of atropisomerism are related to the steric hinderance caused by the bulky isoindole ring. As such, the ground state dihedral in *3-E*-P-R and *3-E*-M-S, for the most stable E isomers, is -87.6° and 86.4° respectively whereas it shifts to 17.2° and 179.5° in the transition states (a-b-c-d in Figure 3.12). Apparently, increasing planarity between the atoms a-b-c-d makes the whole system sterically hindered giving rise to a steric strain. A similar pattern is responsible for the high ΔΔG values in the Z transition states.

Relatively high activation barriers (Table 3.4) for transition of Z-P and Z-M indicate that the interconversion mechanism of the Z isomer does not give very ready access to the formation of its atropisomers. Nearly the same population of *4-Z*-P_R and *4-Z*-M_R isomers as well as the almost equal activation energies of *3-Z*-P-TS and *3-Z*-M-TS in Table 3.3 proves directly the presence of M and P rotamers prior to an interconversion, thereof. On the other hand, lower barrier heights for E-P and E-M conversion and their equally populated fashion convince of a conversion as well as a straight formation.

3.5. Conclusions and Future Work

In this study, cyanoisoindole containing strigolactone analogue, namely strigolactone 3 has been subjected to a computational analysis with quantum mechanical tools. For all isomers of the strigolactone 3, a systematic conformational analysis has been performed. Geometries of P and M conformers of the E and Z isomers as well as their rotational transition state structures have been investigated at the B3LYP/6-31+G(d) level of theory. Further energy refinement has been carried out using M06-2X/-6-31+G(d,p) in solution. Among the four isomers, *3-Z*-P and *3-Z*-M have the lowest relative Gibbs free energies in comparison with *3-E*-P and *3-E*-M isomers. The more stable nature of Z isomers was explained based on the enhanced bifurcating interactions.

Conversion between *3-E*-P-R and *3-Z*-P-R isomers has been considered on two basis: a resonance effect with a partial double bond propensity and a nucleophilic 1,4-addition of OH^- to the alkene center. The former appeared unlikely in terms of energetic considerations. Nevertheless, the latter gave rise to the formation of the more stable

intermediates than E and Z isomers. Hence, equilibrium towards the *3-E*-P-R seems more likely rather than *3-Z*-P-R when starting with the *3-E*-P-R.

Activation energies for the formation of E and Z isomers prove that E and Z isomers are accomplished readily at room temperature. Therefore, E and Z isomers of strigolactone 3 can exist simultaneously in the reaction vessel in the beginning.

The relatively high activation barrier for the atropisomerism of *3-Z*-P to *3-Z*-M or vice versa, due to the hindered rotation ensuing from the bulky isoindole ring proves the existence of P and M structures prior to an interconversion. Nonetheless, these relatively high barriers can be surmounted in time leading into stable Z atropisomers at room temperature.

Lower barrier heights between E atropisomers and their equally populated levels can be attributed to an interconversion of the isomers as well as their direct formation.

In the light of all the above discussion, we deduced that the 45:55 mixture, which is an experimental finding, can be attributed to the presence of both E and Z isomers as both can be formed from strigol 1 with almost the same activation energies. Moreover, it is conceivable to expect an atropisomeric mixture as well.

In order to understand whether a conversion from the E isomer to the more stable Z occurs or not, interconversion of E and Z isomers for the strigol 1 precursor through tautomerization can be investigated in the future.

4. METAL CATALYST EFFECTS IN THE HETERO-DIELS-ALDER REACTIONS

4.1. Introduction

Efficient introduction of diversity into a small molecule is one of the most challenging problems of modern high-throughput organic synthesis. The resulting libraries are expected to increase the probability of identifying new bioactive compounds. Pericyclic reactions are of great importance to the access of complex cyclic or aromatic compounds having biological activity [27-29]. The major classes of pericyclic reactions are cycloaddition reactions associated with multiple bond reduction and new bond formation. In cycloaddition reactions two or more unsaturated molecules combine with the formation of a cyclic adduct. In this reaction there is a net reduction of the bond multiplicity. Sigmatropic rearrangements involve an intramolecular process in which a σ-bond is broken to form an another σ-bond while where a π-bond is converted to a σ-bond in electrocylic reactions (Figure 4.1) or vice-versa.

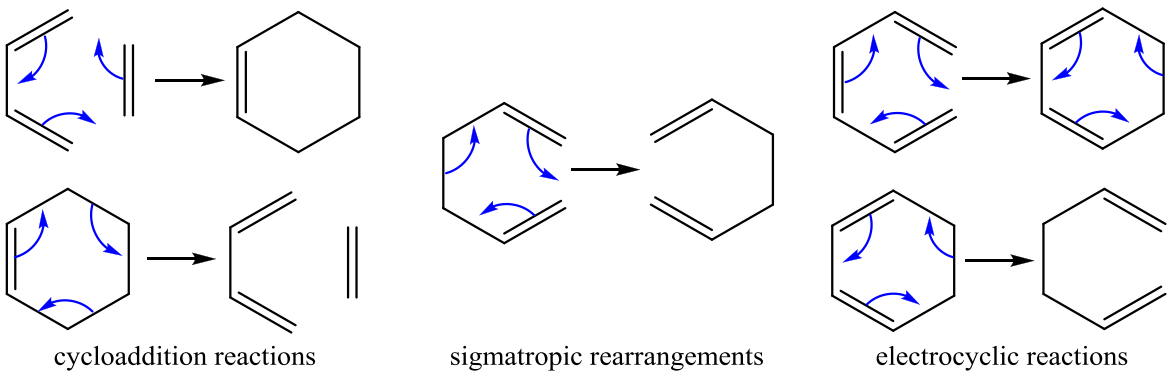

Figure 4.1. Three main classes of pericyclic reactions.

4.2. Diels-Alder Reactions

The most important type of the concerted cycloaddition reactions is the Diels-Alder reaction [4+2] which consists of a diene and dienophile which form a cycloadduct. The Diels-Alder cycloaddition ranks among the best known organic reactions; it is widely used to construct, in a regio- and stereo-controlled way, a six membered ring with up to four stereogenic centers. The versatility of forming two C–C bonds in a concerted fashion explains the enduring interest of the Diels–Alder reaction [30].

In cases where heterocylic rings are involved, besides the normal Diels-Alder reactions the inverse electron demand Diels-Alder (IEDDA) reactions can take place at high temperatures. In a normal Diels-Alder reaction, electrons move from the highest occupied molecular orbital of diene ($HOMO_{diene}$), $HOMO_{diene} \rightarrow LUMO_{dienophile}$, while in an IEDDA reaction a reverse electron motion, $LUMO_{diene} \rightarrow HOMO_{dienophile}$, takes place [31].

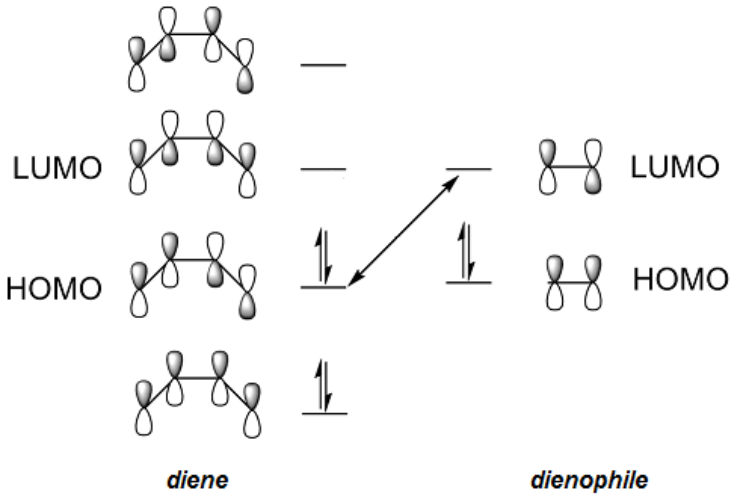

Figure 4.2. Frontier molecular orbital depictions for a normal DA reaction.

4.3. Asynchronicity and Substitution Effect

Diels-Alder reactions of substituted dienes and dienophiles have been found to occur by both concerted and stepwise mechanisms. If both bonds are formed to exactly the same extent in the transition state, this is called a synchronous concerted reaction; otherwise, it is asynchronous [32]. Though some DA reactions are asynchronous, they may

still be concerted with no intermediates located between transition states [33]. In the presence of an asymmetric diene or dienophile, an asynchronous reaction is more notable where the electron rich region of the diene reacts with the electron poor region of the dienophile ensuing from the regioselectivity [34]. However, in an IEDDA reaction the diene and dienophile shift their roles and an adverse inclination towards the electrons comes about.

Besides the asynchronicity of a reaction mechanism, substitution effect plays a crucial role on the prospect of an IEDDA. Introduction of an electron withdrawing group (EWG) to the diene can render it more electron deficient so that an affordable reaction between the more electron deficient diene and electron rich dienophile occurs by facilitating the nucleophilic attack of dienophile to the diene.

Oishi *et al.* reported the IEDDA reactions of 1-substituted phthalazines with enamines or ynamines and found that the expected IEDDA took place resulting in the formation of 1-substituted naphthalenes [35]. Hence, altering the substituent on phthalazine an IEDDA can be controlled and accessibility to the corresponding cycloaddition reaction can be achieved (Figure 4.3).

Anderson *et al*. also disclosed the impact of a C5 substituent on 1,2,3-triazines and participation of 1,2,3-triazines in IEDDA with enamine and ynamine dienophiles even at low temperatures [36]. Thus, IEDDA reactions which usually take place under thermal conditions requiring high reaction temperatures (~120-150°C) can be accomplished under mild conditions by following the above mentioned protocol [37-38].

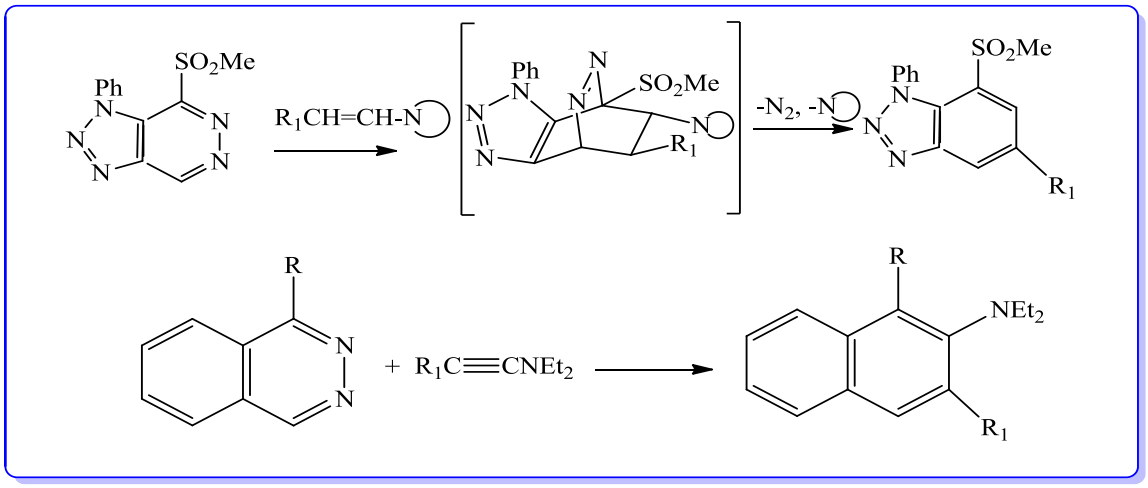

Figure 4.3. Cycloaddition of 1-substituted phthalazine with enamine and ynamine respectively.

4.4. IEDDA of 1,2-Diazines and Siloxy Alkynes

Silicon-functionalized building blocks are finding more and more applications in carbon-carbon bond formation processes. The interest arises not only from the low toxicity, ease of handling, and stability of the silicon-functionalized compounds but also from the increasing number of methodologies available for their synthesis and use in follow-up reactions.

Nevertheless, Hilt *et al.* reported that the use of silicon-functionalized compounds in Diels-Alder reactions is generally restricted to the use of silicon-functionalized dienes since trialkyl-silyl functionalized dienes and dienophiles do not have high activation towards both normal and inverse Diels-Alder reactions [39].

1,2-diazines, also so-called phthalazines, are significant members of heterocylic azadienes providing a broad application of inverse Diels-Alder reactions in the synthesis of complex heterocylic compounds. As pronounced in the previous section, their activity can be enhanced by a variety of substituents. However, reports in the literature display that only a few dienophiles react with unsubstituted phthalazine [40-43].

The work of Wegner *et al.* described the boron based Lewis acid catalyzed IEDDA reactions of 1,2-diazines across a series of dienophiles [44-45]. Moreover, their research

showed that alkynes were unreactive towards unsubstituted phthalazine even in the presence of Lewis acids.

Recently, Rawal *et al.* and Kozmin *et al.* delineated a highly effective silver-catalyzed formal inverse electron-demand Diels-Alder reaction of 1,2-diazines and siloxy alkynes. In accordance with their work, IEDDA reactions can be enhanced by transition metals possessing π acceptor properties like Lewis acids [46].

4.5. Metal Catalyst Effect on IEDDA Reactions

The inverse electron demand Diels-Alder reaction is facilitated pervasively in the presence of Lewis acids or transition metal catalysts in order to enhance the cycloaddition activity when thermal conditions or substitution on the diene/dienophile do not yield a cycloadduct.

The idea of catalysis of IEDDA reactions is based on the Frontier Molecular Orbital (FMO) Theory. The coordination of the catalyst to the diene lowers the energy of lowest unoccupied molecular orbital (LUMO) of the diene compared to the uncatalyzed diene, thus increasing the total charge transfer in the transition state [47].

As such, in the case of bidentate Lewis acid catalyzed 1,2-diazines, a boron-based bidentate Lewis acid can complex with vicinal nitrogen atoms of the 1,2-diazine and facilitates the cycloaddition by lowering the LUMO energy of the 1,2-diazine [44].

Apart from its impact on the FMO and reaction activation, Lewis acids such as $SnCl_4$ were proven to supply only hetero-Diels-Alder products within endo/exo selectivity [33]. Briefly, Lewis acids are capable of altering the shape of the potential energy surface in a hetero-Diels-Alder reaction. On the other hand, it is reported that Lewis acid activation has met with limited access in the case of [4+2] cycloaddition reactions of 1,2-diazine and siloxy alkynes [46]. This shortcoming, however, can be accomplished by developing metal catalysts having high affinity to alkynes. In that regard, transition metals gain attention so as to aid the IEDDA reactions otherwise inaccessible.

Silver-based catalysis is emerging as a novel paradigm in organic synthesis leading to the carbon-carbon bond forming reactions. Kozmin *et al*. proposed that mild silver catalysis is essential for the compatibility with labile siloxy alkynes [48]. Beside the silver, gold precursors were also promoted to ease the cycloisomerization of siloxyl substituted enynes [49].

In this study, we focus on the silver (I) catalyst complexing with bipyridine ligand and its impact on reaction kinetics as well as thermochemical products in IEDDA reactions of 1,2-diazine and siloxy alkyne derivatives (Figure 4.4). At that point, we aim to shed light on the mechanism of 1,2-diazine and siloxy alkyne cycloaddition in the presence of silver catalyst with quantum mechanical tools. To this end, we investigate concerted and stepwise cycloaddition mechanisms as well as complexation reactions. Further, we model substituted 1,2-diazine and siloxy alkynes in order to illuminate the substitution effect on IEDDA of 1,2-diazine and siloxy alkyne.

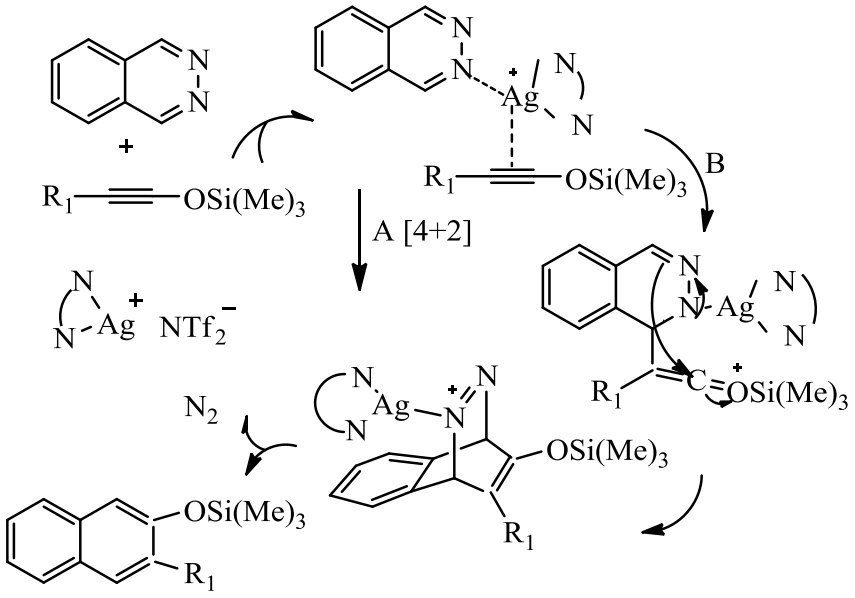

Figure 4.4. 1,2-diazine and siloxy alkyne [4+2] cycloaddition reaction in the presence of silver-bipyridine.

4.6. Methodology

The density functionals that perform best for main-group chemistry are not the same as those that perform best for transition metals [50-52]. Whereas in solid-state chemistry local functionals are often chosen, partly because they are easier to apply to extended systems, in organic chemistry hybrid functionals are the more typical choice because of their demonstrated superior predictions of energetics [53]. Thus far the most popular such hybrid functional is B3LYP, which is a hybrid GGA put together by Stephens *et al.* [54] on the basis of earlier work by Becke and others [9,14,15]. On the other hand, B3LYP is inaccurate in general for transition metals [55].

When studying organometallic catalysis, good accuracy of a chosen functional both in describing main group elements and transition metals is of great importance. The latter seems to perform well with a zero or low Hartree-Fock exchange ($X \leq 15$) whereas the former requires relatively high Hartree-Fock exchange percentage ($X \leq 40$) [56]. The exchange term X is a consequence of inclusion of the Pauli principle ensuing from the necessity of an anti-symmetric wavefuction. The exchange term in effect is a measurement of electron repulsion due to electron exchange [57]. In an effort, Zhao and Truhlar attempted to find the best functional with $X = 0$ [58]. The resulting functional, called M06-L, have the best overall performance of any functional for a combination of thermochemistry, thermochemical kinetics, metallochemical and noncovalent interactions, bond lengths, and vibrational frequencies [59-60].

Another promising approach, not applied to the transition metals pervasively however, involves range-separated functionals [61-67]. Recent research proved that ωB97XD density functional incorporating dispersion corrections shows good performance with small statistical errors compared to standard hybrid functionals [68].

As for the systems involving transition states, functionals optimized by increasing exact exchange percentage into the 40-50% region improve the barrier heights while having an inclination to degrade all other properties [69]. To this end, the most widely used kinetics functional has been mPW1K of Truhlar and coworkers [70].

Relativistic effects are non-negligible for late 3d transition metals, important for 4d transition metals, and so important for 5d transition metals that they must be included for even a zero-order description. For transition metals, a two-component Dirac spinor operator is usually employed. Relativistic effects may be classified into scalar effects and vector effects; the former are due to mass–velocity and Darwin terms in the relativistic kinetic energy, and the latter arise from magnetic interactions involving the operators associated with spin and orbital angular momentum [71].

The main effect of the scalar relativistic term is to shrink the s orbitals and, to a lesser extent, the p orbitals [72-74]. When relativistic effects are to be treated explicitly, all-electron basis sets optimized for such calculations are required for good accuracy. By using ECPs (electron core potential) relativistic calculations can be reduced to a smaller extent by approximating the core electron effects.

If a system becomes a part of a larger system such as metal ligand complexation basis set superposition error is usually inevitable. While the fragment in the larger system utilizes the enhanced description of the basis set, it has a poorer description on its own arising the basis set dependent errors. Therefore, counterpoise corrections provide a corrected interaction energy by describing the basis set of the smaller systems more accurately. The uncorrected interaction energy is

$$V_{AB}(G) = E_{AB}(G,AB) - E_A(A) - E_B(B) \quad (4.1)$$

The counterpoise corrected interaction energy is

$$V_{AB}^{cc}(G) = E_{AB}(G,AB) - E_A(G,AB) - E_B(G,AB) \quad (4.2)$$

where G denotes the coordinates that specify the geometry of the dimer and $E_{AB}(G,AB)$ the total energy of the dimer AB calculated with the full basis set AB of the dimer at that geometry while $E_A(G,AB)$ and $E_B(G,AB)$ denote the total energies of monomers A and B, respectively, computed with the dimer basis set AB at geometry G [24].

4.7. Computational Details

Density functional theory (DFT) was employed within Gaussian09 program package throughout the study. Geometry optimizations and single point calculations were carried out with various hybrid , meta-GGA, local and long-ranged separation functionals in the light of elaborated methods in the methodology.

All geometry optimizations were carried out at the B3LYP/6-311+G(d,p)|SDD level of theory. For Ag(I) the Stuttgart Dresden ECP (SDD) basis set was used whereas 6-311+G(d,p) basis set was used for Si, C, N, O, Cl, H or any other light atoms. In the case of Lewis acids ($SnCl_4$) SDD basis set was used for Sn metal as well. For model reactions in the first place, 6-31+G(d) basis set was chosen for practicality. However, increasing the size of the basis set from 6-31+G(d) to 6-311+G(d,p) considerably refined the Gibbs free energies of activation.

B3LYP structures proved similar geometries with those of M06-L. However geometry optimizations with M06-L yielded late transition states particularly in the case of substituted diazines and siloxy alkynes. Thus, M06-L has been taken into consideration for only single point calculations on B3LYP optimized geometries. Beside this functional, mPW1K and ωB97XD were also employed so as to incorporate kinetic density and dispersion corrections relevant to noncovalent interactions into energetic considerations.

Polarizable continuum model (PCM) solvation effects were included via single point calculations. Dichloromethane was implemented as the solvent according to the reaction conditions in PCM calculations.

In calculating the activation energies, reactants were taken into account separately via a bimolecular reaction as well as a unimolecular reaction resulting from quaternary complexes of Ag(I) with both diazine and siloxy alkyne. The thermodynamic nature of reactants and products were endorsed with IRC calculations.

5. RESULTS AND DISCUSSION

5.1. Proposed Reaction Mechanisms

5.1.1. Complexation Reactions with Model Compounds

A series of experimental studies regarding the characterization of Ag(I) revealed that the use of bidentate chelating ligands proved beneficial effect on the IEDDA reaction of 1,2-diazine and siloxy alkyne [46]. Reports in literature exhibit that the coordination number of Ag can vary in a range of 2 to 6 [75-76]. In this study, we focused on the 2,2'-bipyridine as bidentate chelating N-donor ligands.

In the absence of Ag(I), 1,2-diazine and siloxy alkyne cycloaddition is simply anticipated to take place via a concerted mechanism. Thus, our first attempt was to investigate the complexation of 1,2-diazine and siloxy alkyne with Ag(I) separately. To this end, using silver ethylenediamine for the coordination of Ag(I) and methoxy alkyne as model chemicals, we modeled silver-diazine complex and silver-alkyne complex as depicted in Figure 5.1 and Figure 5.2 respectively. In addition, we assumed the dimeric $Ag_2(\mu\text{-phtz})_2$ unit in which case a tetradentate coordination of Ag(I) bridged by two diazine units was achieved and resulted in a six-member ring complex (Figure 5.3).

The bidentate nature of the diazine similar to the ethylenediamine or bipyridine in the real reaction medium does not necessarily lead to the bifurcating coordination of Ag(I) with the vicinal diazine nitrogens albeit it can be anticipated in the case of bidentate ligands. Seemingly, Ag(I) did not coordinate with both diazine nitrogens but only with either of them. This behavior can be elucidated on the basis of face away lone pairs of N-donors rather than chelating. Therefore, only one N-donor is available to share its lone pair electrons.

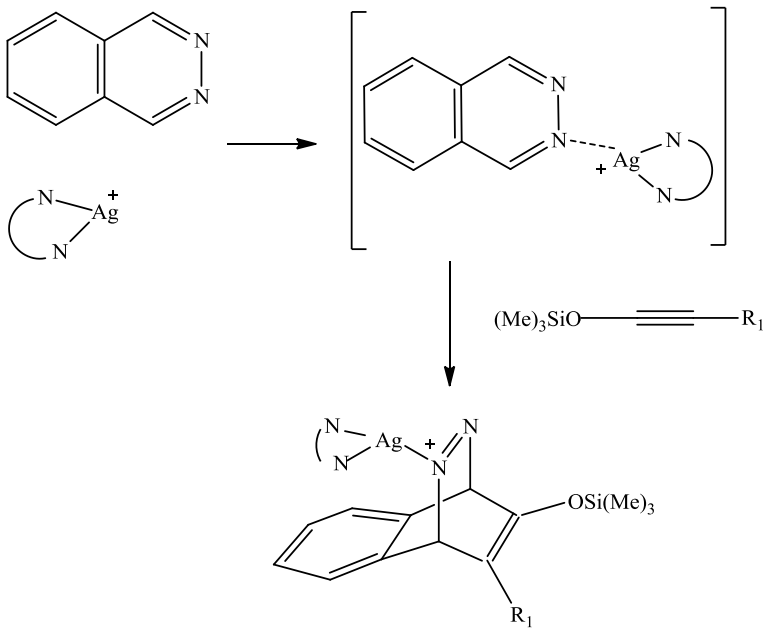

Figure 5.1. [4+2] cycloaddition of 1,2-diazine and siloxy alkyne upon silver diazine complex formation.

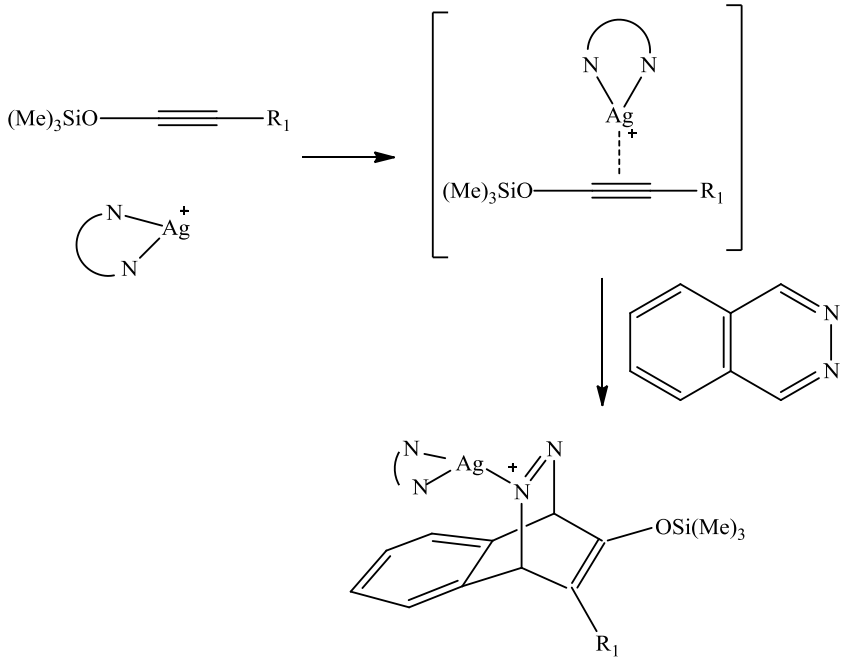

Figure 5.2. [4+2] cycloaddition of 1,2-diazine and siloxy alkyne upon silver alkyne complex formation.

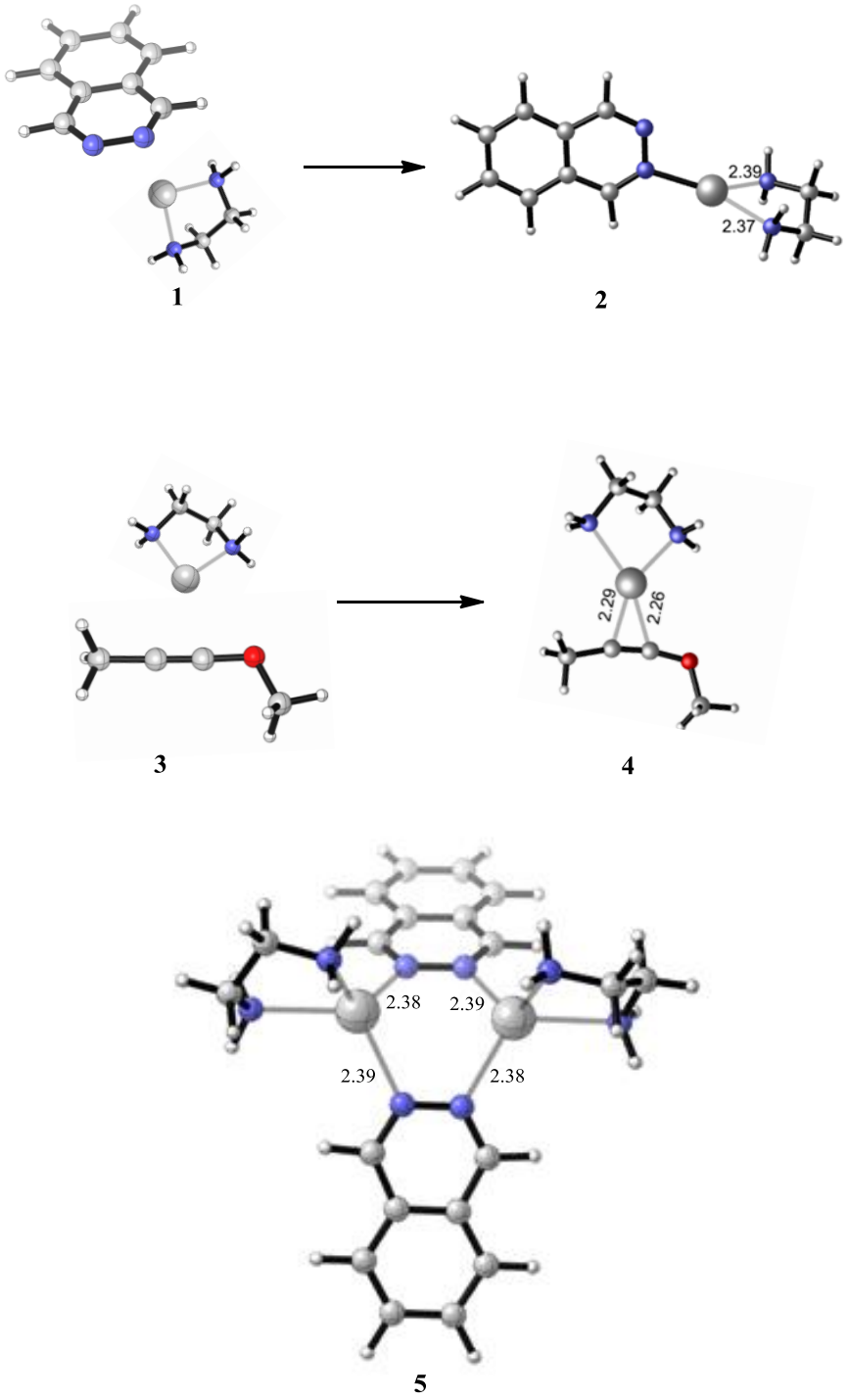

Figure 5.3. Silver-ethylenediamine and diazine complexation (1→2) and silver-ethylenediamine and methoxy alkyne complex formation (3→4) (B3LYP/6-31+G(d)). $Ag_2(\mu\text{-phtz})_2$ (5) dimer complex (B3LYP/6-31+G(d)).

Table 5.1. Reaction energies (kcal/mol) of possible complexes in the presence of Ag(I) (B3LYP/6-31+G(d)).

Complex	ΔH_{rxn}	ΔG_{rxn}
2	-33.4	-24.7 (-23.4)
4	-25.7	-14.8 (-14.3)
5[(a)]	35.3	48.1
5[(b)]	-31.5	-1.36

[(a)] Both silver-diamine diazine complexes were considered as reactants. [(b)] Reactants were taken into account separately. Counterpoise corrected energies are displayed in parenthesis.

The silver-ethylenediamine and diazine complex (2) is more favorable in comparison to silver-ethylenediamine and methoxy alkyne complex (4) (Table 5.1). Besides, the dimeric $Ag_2(\mu\text{-phtz})_2$ (5) is not favored based on rather high Gibbs free energies presumably related to the decreased entropy of the system.

5.1.2. Complexation Reactions of 1,2-Diazine and Siloxy Alkyne with Ag(I)-bipyridine

Ag(I) coordinated with bidentate N-donors seems to prefer existing in the form of silver-diazine complex. On the other hand, this behavior of Ag(I) can depend on the nature of the bidentate ligand as well as the methodology in terms of computational viewpoint. To further ascertain the exact nature of the equally likely complexes, we continued with the bipyridine as a chelating ligand and siloxy alkyne which replaced methoxy alkyne.

Two possible complexes of silver with the diazine and siloxy alkyne (Ag(I)-bipyridine diazine and Ag(I)-bipyridine siloxy alkyne respectively) are depicted in Figure 5.4. In both cases, silver demonstrates propensity to a ternary complex formation.

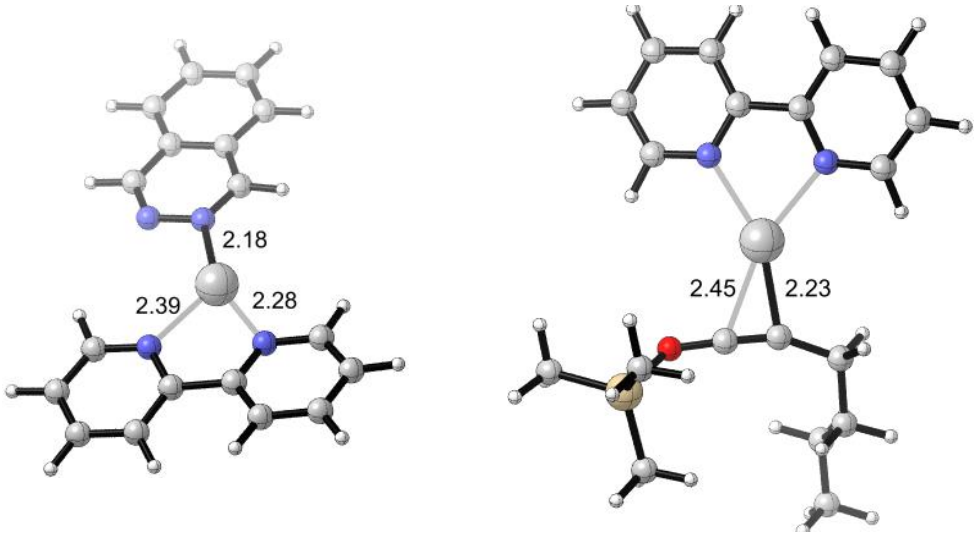

6 **7**

Figure 5.4. Ag(I)-bipyridine diazine (6) and Ag(I)-bipyridine siloxy alkyne (7) complexes (B3LYP/6-311+G(d,p)).

Table 5.2. Complex formation energies (kcal/mol) for 6 and 7.

B3LYP/6-311+G(d,p)		
Complex	ΔH_{rxn}	ΔG_{rxn}
6	-38.2	-28.7
7	-31.4	-21.0
M06-L/6-311+G(d,p)		
Complex	ΔH_{rxn}	ΔG_{rxn}
6	-40.2	-30.6
7	-37.4	-25.4
M06-L/6-311+G(d,p)//B3LYP/6-311+G(d,p)		
Complex	ΔH_{rxn}	ΔG_{rxn}
6	-42.2	-32.6
7	-40.4	-30.0

Table 5.2. Complex formation energies (kcal/mol) for 6 and 7. (contd.)

M06-L/6-311+G(d,p)//B3LYP-6-311+G(d,p)[a]		
Complex	ΔH_{rxn}	ΔG_{rxn}
6	-24.3	-14.8
7	-25.8	-15.3
ωB97XD/6-311+G(d,p)//B3LYP-6-311+G(d,p)		
Complex	ΔH_{rxn}	ΔG_{rxn}
6	-43.2	-33.7
7	-41.4	-31.0
ωB97XD/6-311+G(d,p)//B3LYP-6-311+G(d,p)[a]		
Complex	ΔH_{rxn}	ΔG_{rxn}
6	-25.3	-15.8
7	-26.8	-16.4
MPW1K/6-311+G(d,p)//B3LYP/6-311+G(d,p)		
Complex	ΔH_{rxn}	ΔG_{rxn}
6	-42.0	-32.4
7	-39.4	-29.0
MPW1K/6-311+G(d,p)//B3LYP/6-311+G(d,p)[a]		
Complex	ΔH_{rxn}	ΔG_{rxn}
6	-23.0	-13.4
7	-23.5	-13.1

[a] PCM solvent corrections in dichloromethane.

From Table 5.2 gas phase optimized structures prove that Ag(I)-bipyridine diazine complex is more stable than Ag(I)-bipyridine siloxy alkyne complex whereas in dichloromethane this non-negligible difference almost vanishes or slightly reverses depending on the methodology. However, experimental studies upon characterization of Ag(I) prompt us to carry on with the Ag(I)-bipyridine diazine which is subject to a nucleophilic attack of siloxy alkyne [46].

5.1.3. Concerted versus Stepwise Mechanism with Model Compounds

In this section we have modeled the cycloaddition reaction between the alkyne and the Ag(I)-diazine complex (Figure 5.5). Considering the nature of heterodiazines and asymmetric dienophiles, the possibility of a stepwise reaction mechanism was taken into consideration. In a stepwise mechanism, a highly reactive ketenium formation was expected as an intermediate (as previously depicted in Figure 4.4). The comparison of the potential energy surfaces of the concerted and the stepwise mechanisms was carried out to determine the most viable reaction path.

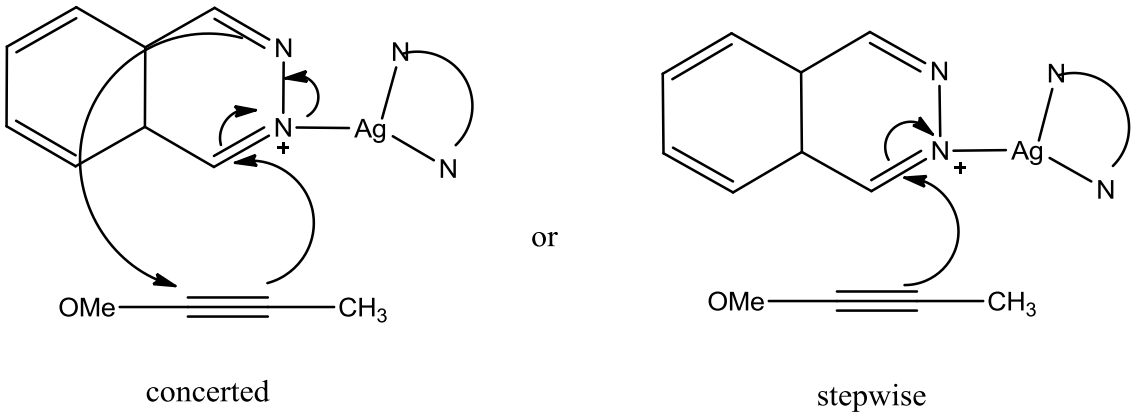

Figure 5.5. Overview of concerted and stepwise mechanisms for 1,2-diazine and methoxy alkyne cycloaddition in the presence of Ag(I)-ethylenediamine.

No intermediate was observed through downhill pathway calculations (Figure 5.6). In the case of *stepwise* cycloaddition TS_2, C-C-O bond angle near linear (170.2°) in the methoxy alkyne can be attributed to a momentary ketenium. Thus, we still observe a concerted but asynchronous reaction mechanism.

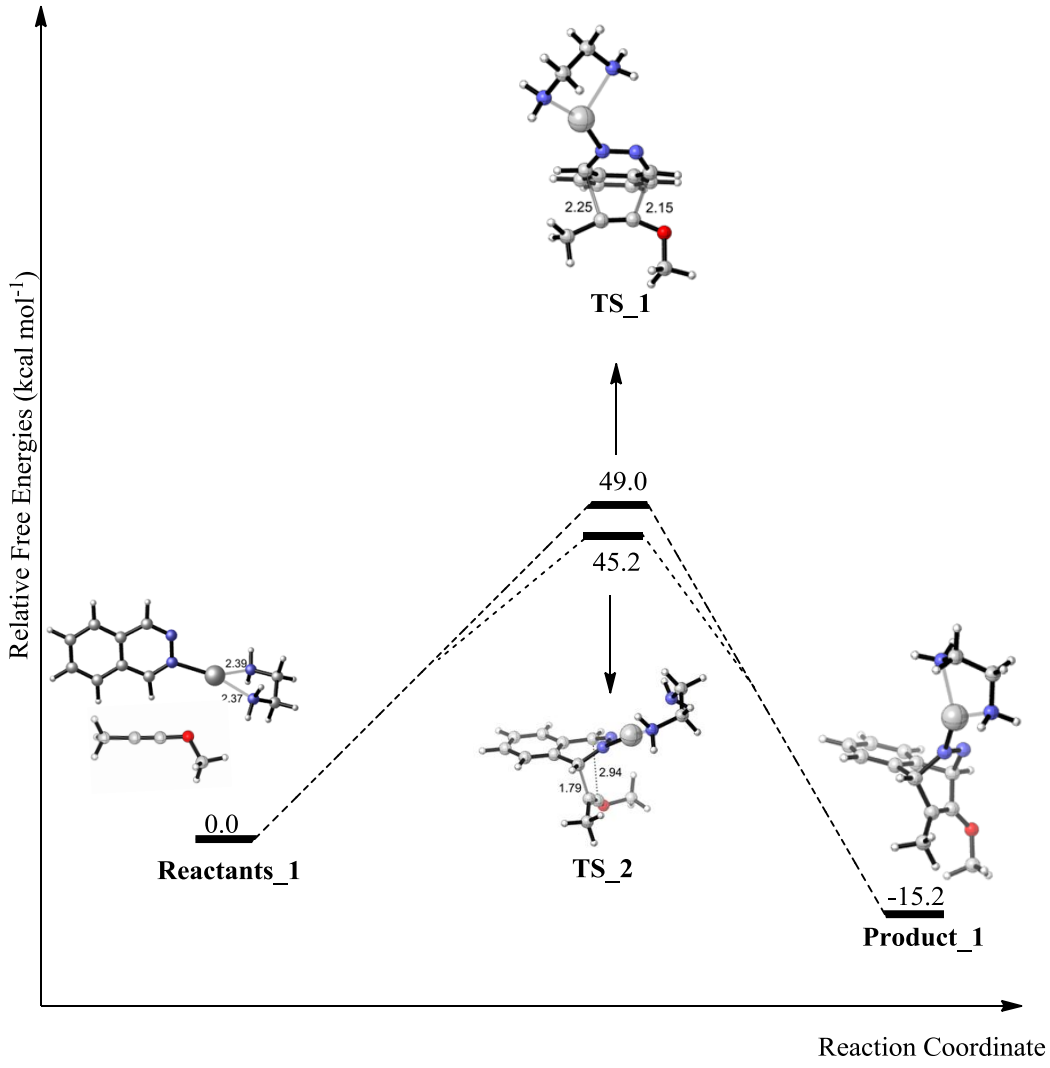

Figure 5.6. Gibbs free energies of activation (kcal/mol) for the proposed concerted (TS_1) and stepwise mechanisms (TS_2) and product formation (Product_1) through IRC (B3LYP/6-31+G(d)).

5.1.4. Mechanism of 1,2-Diazine and Siloxy Alkyne Cycloaddition

In the case of 1,2-diazine and siloxy alkyne we contemplated two possible reaction mechanisms. In an effort, we modeled the cycloaddition reaction on two bases: a nucleophilic attack of siloxy alkyne to silver-bipyridine diazine complex (6) and a nucleophilic attack of diazine to silver-bipyridine siloxy alkyne complex (7).

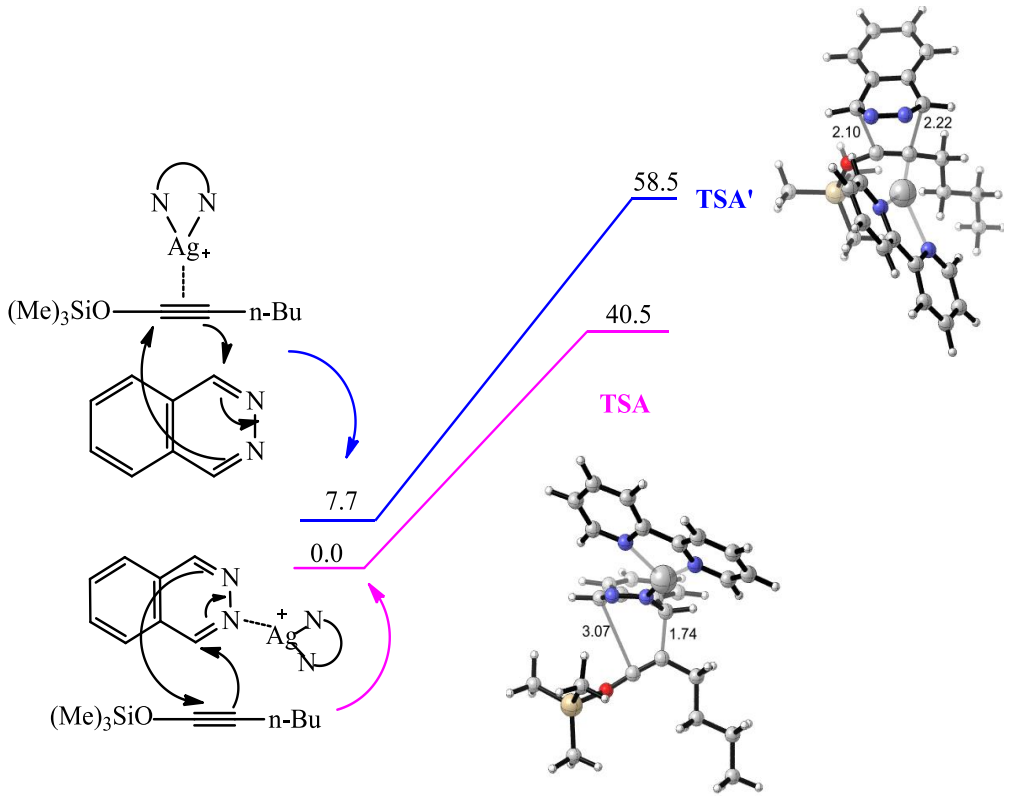

Figure 5.7. Transition state structures of 1,2-diazine and siloxy alkyne cycloaddition. Relative Gibbs free energies (kcal/mol) (B3LYP/6-311+G(d,p)).

From Figure 5.7, the activation barrier of the mechanism through the TSA is 40.5 kcal/mol while that of the mechanism allowing to TSA' is 50.8 kcal/mol. Relatively lower activation energy in the case of a nucleophilic attack of siloxy alkyne to the silver-bipyridine diazine complex leading to the TSA with a $\Delta\Delta G^{\pm}$=10.3 kcal/mol proves the reaction pathway via the nucleophilic attack of siloxy alkyne to the initially formed silver-bipyridine diazine complex. In addition, 1.74 and 3.07 Å bond lengths in the case of TSA exhibit an appreciably asynchronous mechanism whereas for TSA' a synchronous mechanism with almost equal contributions of both carbon atoms corresponding to 2.10 and 2.22 Å bond lengths appear. Despite the asynchronicity, the reaction is still concerted for TSA.

5.2. Regioselectivity of 1,2-Diazine and Siloxy Alkyne Cycloaddition

Asymmetric dienophiles such as siloxy alkyne, tend to attack from the electron rich site in a formal inverse electron demand Diels-Alder reaction. We have thus aimed to unravel the reactive site in an asymmetric siloxy alkyne in its cycloaddition reactions with 1,2-diazines (Figure 5.8).

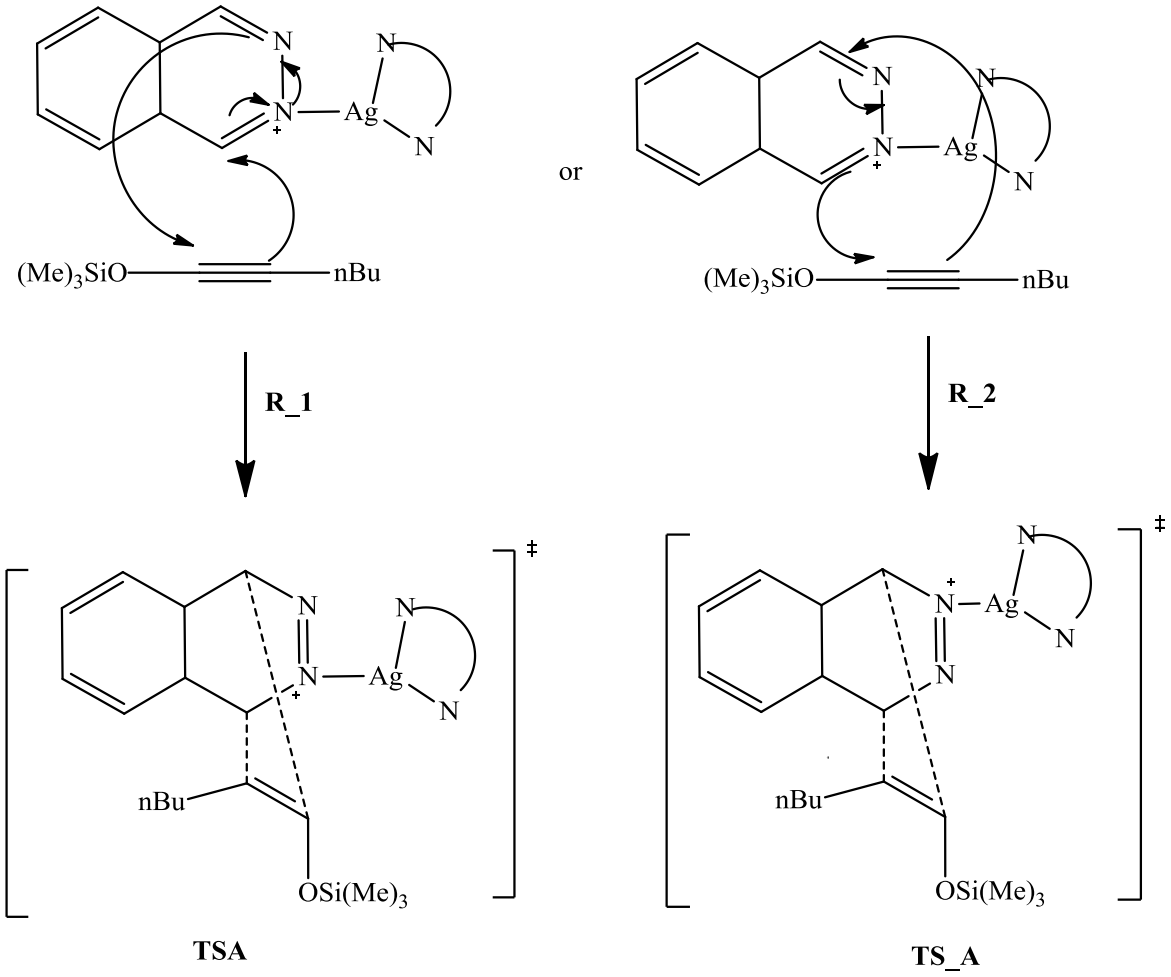

Figure 5.8. Regioselectivity for the cycloaddition of siloxy alkyne and silver-bipyridine diazine complex.

TSA and TS_A represent two different transition state structures with the alternate reaction sites. The Mulliken charge for the C3 with -0.569 charge in TSA was -0.508 before the nucleophilic attack of siloxy alkyne and that of the alkyne carbon possessing previously 0.717 increased to 0.824 (Figure 5.9 and Table 5.3). These resulting charge

patterns prove the charge transfer from one species to the other. Seemingly, the reason for the charge increase in C2 of alkyne strongly interacting with the complex 6 can be associated with a diminishing electron density being transferred to the 6. In a similar sense, the Mulliken charge of the C3 in TS_A decreased from -0.508 to -0.682 indicating a charge transfer from the electron rich alkyne to the silver-bipyridine diazine complex.

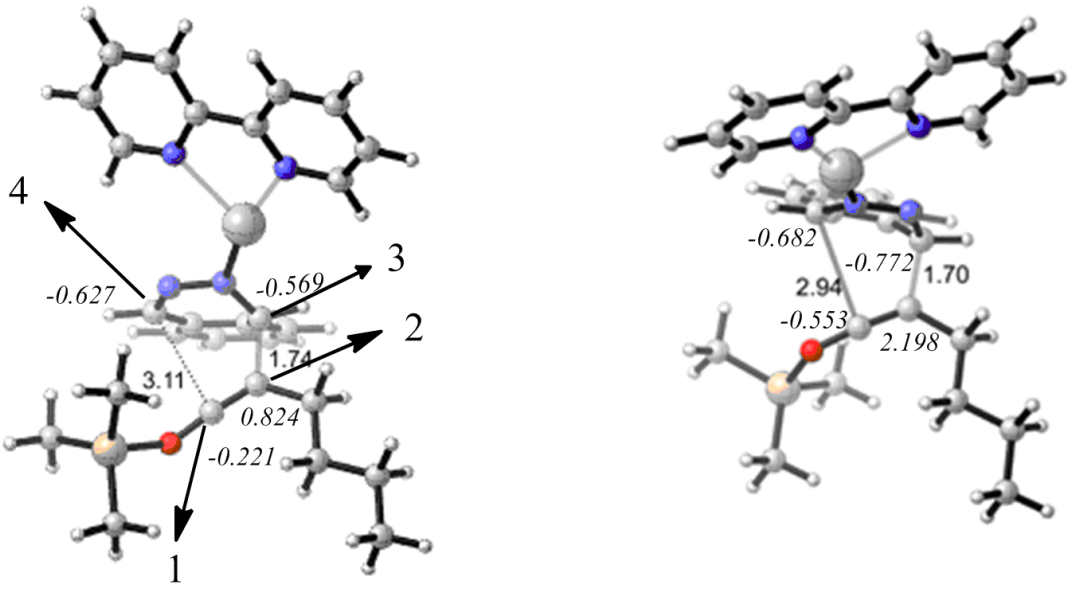

TSA
(44.7)

TS_A
(47.5)

Figure 5.9. Gibbs free energies of activation (kcal/mol) for siloxy alkyne and silver-bipyridine diazine complex cycloaddition (B3LYP/6-31+G(d)). Mulliken charges are presented in italics.

Table 5.3. Mulliken charges of atoms of silver-bipyridine diazine complex and siloxy alkyne (B3LYP/6-31+G(d)).

	C1	C2	C3	C4
silver-bipyridine diazine	-	-	-0.508	-0.505
siloxy alkyne	-0.073	0.717	-	-

As for the difference between TSA and TS_A, the alternating reaction sites bring about more preferential TSA in terms of activation energies (44.7 kcal/mol for TSA and

47.5 kcal/mol for TS_A). In the case of TSA, C2 and C3 as well as C1 and C4 which correspond to electron deficient site on siloxy alkyne and electron rich site on silver-bipyridine diazine or vice versa, exhibit a stronger interaction whereas C1 and C3 weak interaction in the case of TS_A ensues from a less favorable charge transfer.

We checked the charge distribution of reactants in more detail so as to determine the shift of electron distribution of silver-bipyridine and diazine separately in the silver-bipyridine diazine complex distorted as a result of complex formation. Natural population analysis (NPA) displayed that upon complexation of silver-bipyridine with the 1,2-diazine a charge transfer from 1,2-diazine to the silver-bipyridine acting as a Π acceptor takes place. As we carried out geometry optimizations at the B3LYP/6-311+G(d,p)|SDD for further analysis, we took the calculated charge into account at this level of theory.

Table 5.4 illustrates the charge variance when electron acceptor silver-bipyridine due to posing a cationic property permits the electron flow from the diazine to itself and thus resulting in a decreasing charge (0.86) in the silver-bipyridine though the overall charge does not change. From the viewpoint of diazine, initially neutral diazine species has a positive charge (0.14) emanating from donation of electrons.

Table 5.4. NPA charges of silver bipyridine and diazine both in complex and as isolated reactants at B3LYP/6-311+G(d,p).

	Silver-bipyridine	1,2-diazine	Silver-bipyridine in complex 6	Diazine in complex 6
NPA	1	0	0.86	0.14

5.3. Catalyzed versus Uncatalyzed Cycloaddition of 1,2-Diazine and Siloxy Alkyne

In order to understand the silver catalyst effect on 1,2-diazine and siloxy alkyne cycloaddition (Figure 4.4), we pursued a comparative study of the catalyzed and uncatalyzed cycloaddition reactions. The Ag(I) catalyzed reaction profile is depicted in Figure 5.10. In the first place, we have qualitatively taken the activation energies into consideration when comparing the two reaction pathways. As seen from the energy

profiles, barrier heights are too high to enable the cycloaddition at room temperature. Thereby, we further changed our methodology in computing energetics (in section 5.4, Table 5.6). Catalysis of the 1,2-diazine and siloxy alkyne in the presence of Ag(I) thus endorses the cycloaddition by 8 kcal/mol difference in comparison to the uncatalyzed reaction (Figure 5.11). However, the catalyst doesn't alter the shape of the potential energy surface where both pathways end up with the silyl protected naphthalene. Nitrogen gas release occurs favorably with an increasing entropy and so yielding remarkably stable products P_A-II and P_B-II (Figure 5.10 and 5.11) by decreasing the Gibbs free energy of reaction. We came to that conclusion via IRC calculations implemented for both reaction pathways.

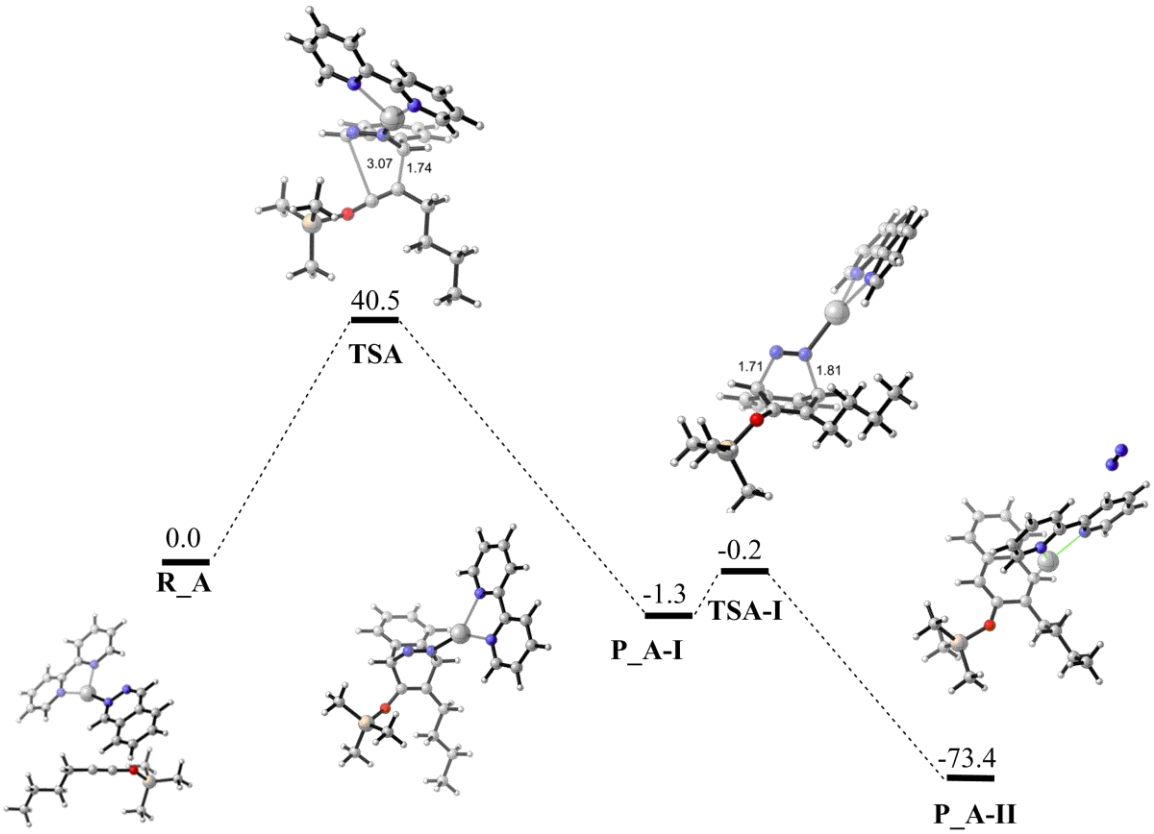

Figure 5.10. Relative free energy profile (kcal/mol) for the Ag(I) catalyzed cycloaddition (B3LYP/6-311+G(d,p)).

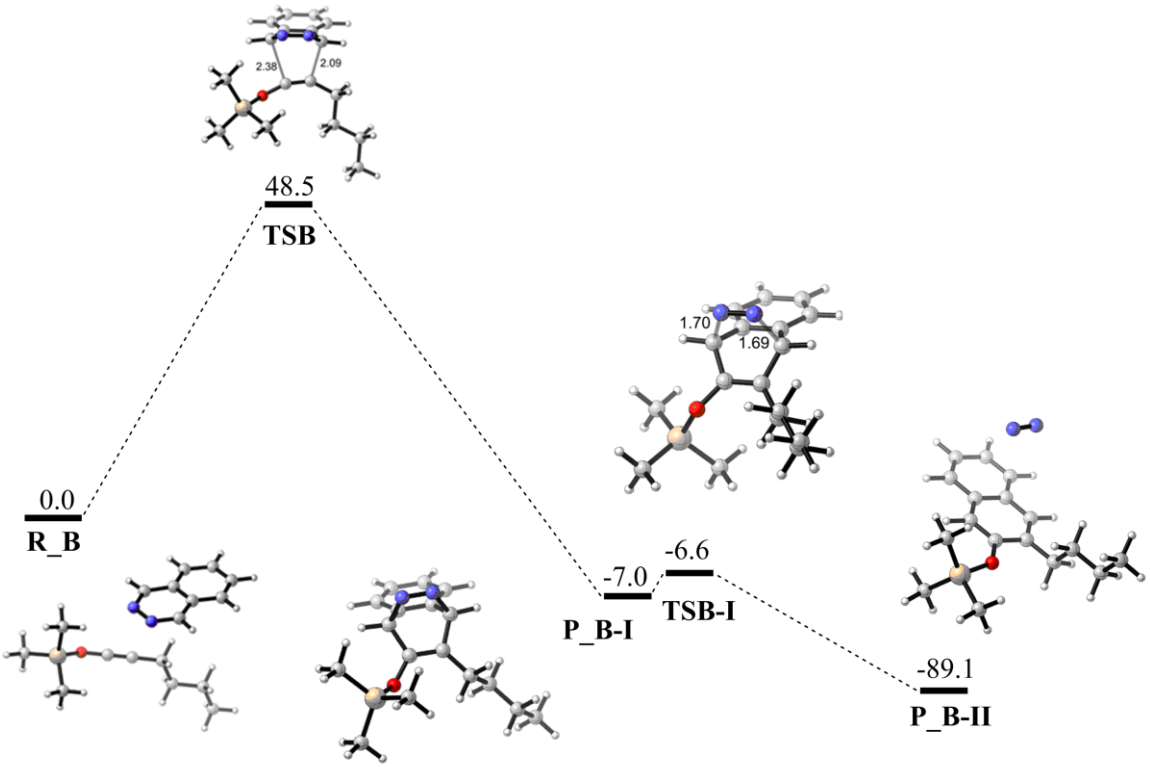

Figure 5.11. Relative free energy profile (kcal/mol) for the uncatalyzed cycloaddition (B3LYP/6-311+G(d,p)).

Once we proved that the Ag(I) catalyst favored the cycloaddition reaction of 1,2-diazine and siloxy alkyne, we proceeded through a Lewis acid effect on the cycloaddition reaction of interest.

5.3.1. Lewis Acid Catalyzed 1,2-Diazine and Siloxy Alkyne Cycloaddition

Lewis acids are known to have strong Π acidic properties and enable to alter the shape of potential energy surface by reversing the reaction mechanism in some cases. Apart from that, they tend to lower the activation barriers and render the otherwise thermal cycloaddition reactions likely even at room temperature. In this respect, we considered the Lewis acid effect on the [4+2] IEDDA reaction of 1,2-diazine and siloxy alkyne (Figure 5.12). In doing so, we aimed to elicit the similarities or differences between Ag(I) catalysis and $SnCl_4$ as a model Lewis acid catalyst. We sought the consistency with the previously explored experimental data.

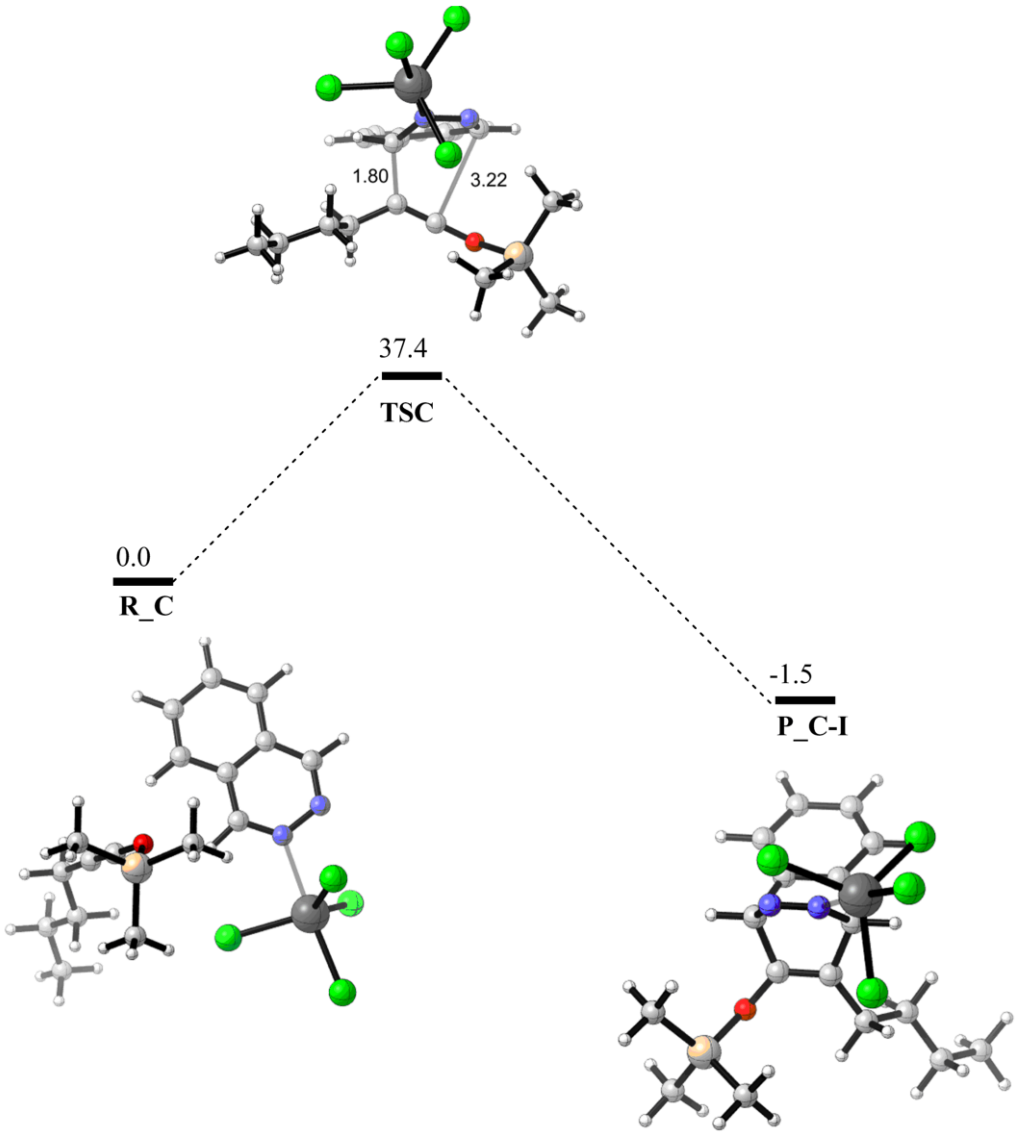

Figure 5.12. Relative free energy profile (kcal/mol) of $SnCl_4$ catalyzed 1,2-diazine and siloxy alkyne cycloaddition (B3LYP/6-311+G(d,p)).

On the basis of a qualitative analysis, $SnCl_4$ appears to enable the required activation and produce the expected cycloadduct. On the other hand, it has relatively lower activation energy than the Ag(I) catalyzed cycloaddition which underlines a discrepancy with the experimental results. To further inspect this unexpected outcome and so as to set up a more realistic picture of the activation energies we continued to perform the energy calculations of the B3LYP/6-311+G(d,p)|SDD optimized transition state structures as well as the reactants with MPW1K, M06-L and ωB97XD level of theory (in the following

section in Table 5.6) by accounting for kinetic density, noncovalent interactions and dispersion forces.

5.4. Substitution Effect on 1,2-Diazine and Siloxy Alkyne Cycloaddition

Substituent role in both normal DA and IEDDA reactions has been the subject of extensive studies in construing the reactivity of dienes and dienophiles. The introduction of an electron withdrawing group to the electron deficient diene in IEDDA reactions promotes the electron deficiency and renders it more reactive towards electron rich dienophiles. Likewise, electron donating groups encompass an increase in the electron density of diene and less reactivity towards dienophiles arises. Beside diene substitution, substituted dienophiles can also enhance reactivity or else can refrain in an adverse effect. In order to foster the IEDDA reaction of 1,2-diazine and siloxy alkyne, Ag(I) catalysis has worked as a sufficient tool, however devising unprecedented models as protected aromatic compounds can be expanded. Thus, in order to explain the prominent role of substitution on IEDDA and rationalize the reaction mechanism on the basis of substitution effect, we viewed substituted diene and dienophiles (Figure 5.13 and Table 5.5).

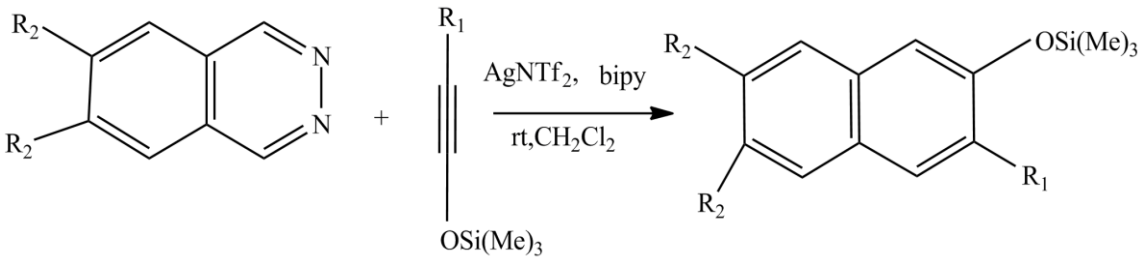

Figure 5.13. Scope of substituent effect on Ag(I) catalyzed cycloaddition reactions.

As seen from Figure 5.14, transition state geometries for three different structures are alike though they energetically differ that we dwell on the details in Table 5.6. Similar to the unsubstituted TSA, we observed an asynchronous but concerted reaction mechanism. IRC calculations verified the substituted cycloadduct formation for three cases as well. The strong vibrational frequency associated with the shorter bond distance (1.75-1.76 Å) points out a late transition state whereas a bond distance around ~3 Å emphasizes

an early interaction and elucidates the lower activation barriers in comparison to the uncatalyzed cycloaddition.

Table 5.5 Experimental results [46] of 1,2-diazine and siloxy alkyne cycloaddition.

Entry	R_1	R_2		Catalyst	Time (h)	Yield
A	n-butyl	H	H	$AgNTf_2$	2	82
B	n-butyl	H	H	-	-	-
C	n-butyl	H	H	$SnCl_4$	-	-
D	n-butyl	CH_3	CH_3	$AgNTf_2$	3	84
E	CH_3	H	H	$AgNTf_2$	3	73
F	CH_2CH_2Ph	H	H	$AgNTf_2$	1	70

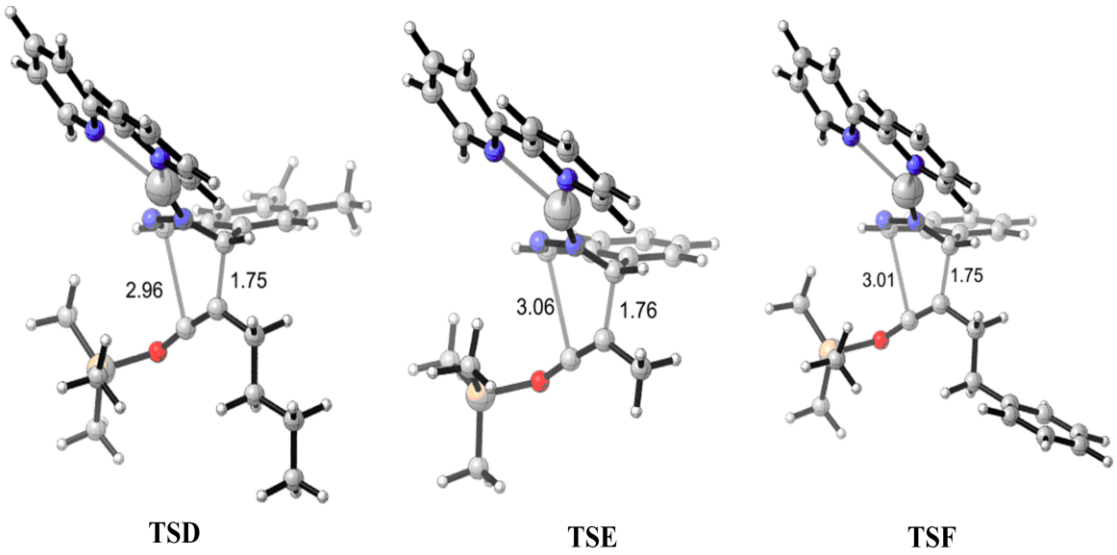

Figure 5.14. Substituted 1,2 diazine and siloxy alkyne transition state structures optimized (B3LYP/6-311+G(d,p)).

Table 5.6. Gibbs free energy of activation (kcal/mol) for six different model reactions.

	TSA	TSB	TSC	TSD	TSE	TSF
MPW1K/6-311+G(d,p)// B3LYP/6-311+G(d,p)	24.2	31.6	22.8	27.2	30.0	23.2
MPW1K/6-311+G(d,p)// B3LYP/6-311+G(d,p)[a]	26.6	31.5	21.0	29.2	32.3	26.0
M06-L/6-311+G(d,p)// B3LYP/6-311+G(d,p)	25.9	34.4	18.7	29.0	31.1	24.4
M06-L/6-311+G(d,p)// B3LYP/6-311+G(d,p)[a]	28.4	34.3	16.9	33.1	35.4	27.4
ωB97XD /6-311+G(d,p)// B3LYP/6-311+G(d,p)	25.7	33.3	18.6	28.4	31.6	20.9
ωB97XD /6-311+G(d,p)// B3LYP/6-311+G(d,p)[a]	28.2	33.3	16.4	30.5	34.0	26.8

[a] Polarizable Continuum Model solvent corrections in dichloromethane.

Single point calculations at three different methods apparently improved the activation energies and thereby providing cycloaddition reactions which are possible at room temperature in the presence of Ag(I) as well as $SnCl_4$ (Table 5.6). On the other hand, still high barrier energies for the uncatalyzed cycloaddition (~31-34 kcal/mol) corresponding to TSB are not probable to surmount at room temperature. As for the substituted transition structures, introduction of the electron donating methyl groups to the diazine seen in TSD, rises the activation energies compared to the TSA. The primary reason for this occurrence develops from the diminishing reactivity of methyl substituted diazine towards the siloxy alkyne. TSE also displays higher barrier heights due to the replacement of the n-butyl to the methyl group located on the siloxy alkyne. Since siloxy alkyne acts as a nucleophile in this cycloaddition reaction, displacing long alkyl chain destabilizes the siloxy alkyne by reducing its nucleophilic nature. Rather the reverse fashion is encountered for the aryl substituted ethyl on the siloxy alkyne not only because electron delocalization on the phenyl ring stabilizes the TSF but also endorsing the nucleophilic attack of the siloxy alkyne.

In general, solvation energies exhibit a higher trend than the gas phase energies except TSC from Table 5.6. The reason for seeing higher activation barriers in dichloromethane can be ascribed to the fact that solvent accessible area is filled with the

dichloromethane in solvated models, and this hinders the accessibility of the siloxy alkyne to the 1,2-diazine complexed with Ag(I). We came to this conclusion from the increasing free energies of transition states and reactants in dichloromethane.

5.5. Molecular Orbital Analysis

After modeling the prototype reactions of substituted 1,2-diazine and siloxy alkynes and probing the effect of catalyst itself as well as with the substitution of the reactants on the activation barriers indirectly related to the reaction rates on the basis of chemical kinetics, we elaborated the motives of the uncatalyzed and catalyzed IEDDA reactions through a molecular orbital analysis approach.

In Figure 5.15, the smaller energy gap (0.509 eV) between the HOMO of siloxy alkyne and LUMO of silver-bipyridine diazine (6) with respect to the uncatalyzed cycloaddition (4.00 eV) invokes the significant role of a catalyst in otherwise unlikely IEDDA reactions. The contribution of Ag(I) herein is literally to facilitate the HOMO-LUMO overlap by lowering the energy between two frontier molecular orbitals. As seen from I and II (Figure 5.15), LUMO of Ag(I) complexed diazine possesses a lower LUMO energy bringing it to the proximity of the HOMO of siloxy alkyne.

Substituted siloxy alkyne derivatives can also afford an IEDDA reaction in the presence of Ag(I) by lowering the energy gap between LUMO of diazine and HOMO of alkyne (Figure 5.15). Therefore, substitution can facilitate a diversity of silyl protected naphthalene derivatives.

Relatively lower HOMO-LUMO gap (V) in Figure 5.15 for the $SnCl_4$ catalyzed 1,2-diazine and siloxy alkyne supports the lower activation energies (Table 5.6) seen in the case of $SnCl_4$ catalysis. The lower LUMO of $SnCl_4$ complexed 1,2-diazine ranks the most efficient way among all studied models throughout this study. Herein, empty p orbitals of the Sn seems more available to accept electrons from N-donor of diazine relative to the Ag(I) which takes on its Π acceptor property from its cationic nature leading the most stable d^{10} configuration.

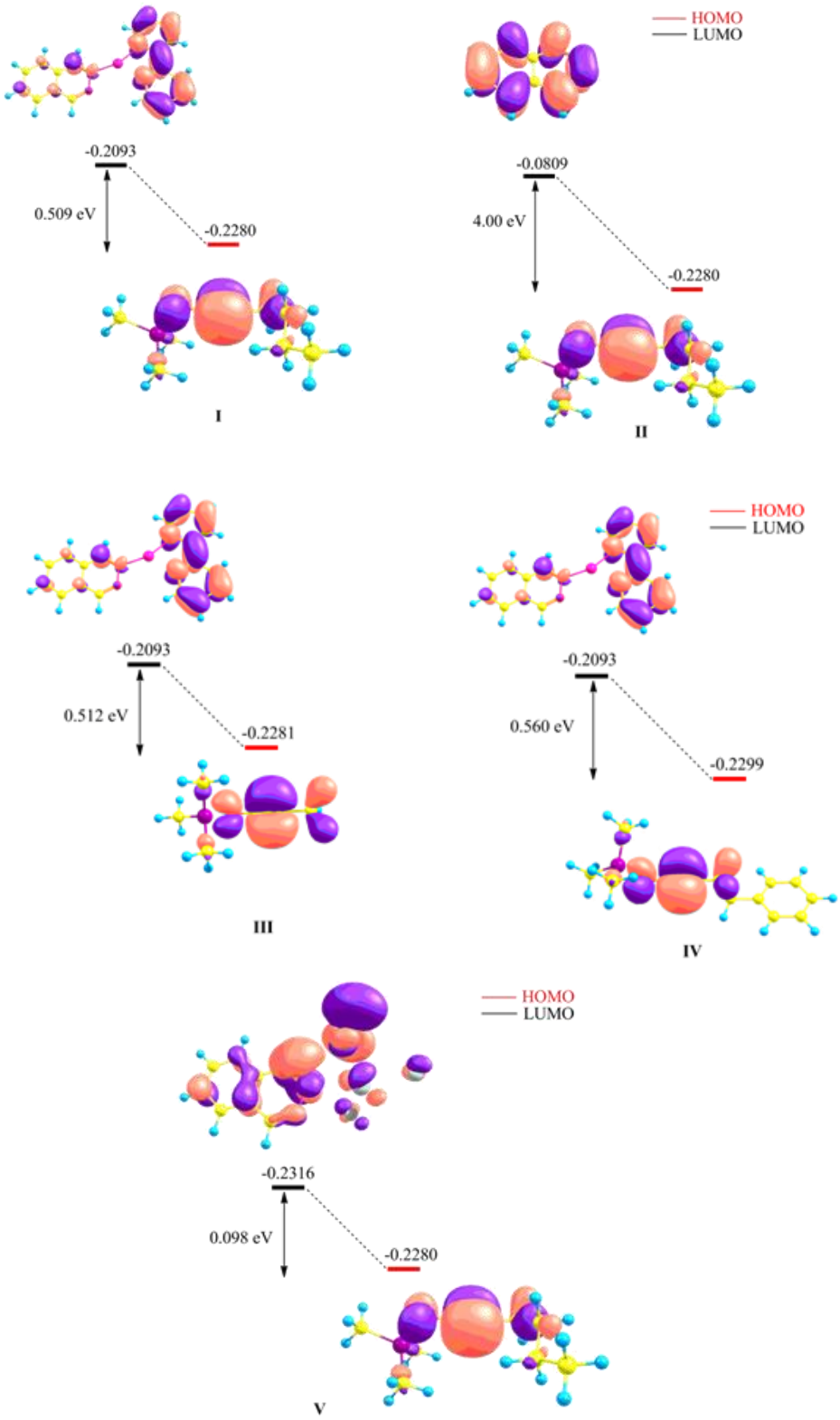

Figure 5.15. HOMO-LUMO energy profile of the Ag(I) catalyzed (I, III, IV), uncatalyzed (II) and $SnCl_4$ (V) catalyzed cycloaddition (Entries A, B, E, F, C respectively in Table 5.5). Energy gaps between HOMO and LUMO (in eV) (B3LYP/6-311+G(d,p)).

5.6. Conclusions

In this study, we focused on the Ag(I) catalysis which was experimentally proven to enhance the IEDDA reaction of 1,2-diazines and siloxy alkynes. Initially, we investigated the possible complexes emerging as a consequence of the affinity of Ag(I)-bipyridine to both 1,2-diazine and siloxy alkyne. In doing so, we determined the most stable complex. We began with the Ag(I)-ethylenediamine, in the first place using a smaller bidentate N-donor ligand. Afterwards, we carried on with bipyridine ligand to be consistent with the experiment in addition to regarding the contribution of the aromacity. In order to warrant the reproducibility of the calculated results, we performed our computations across a range of methodology. As a result, we concluded that silver-bipyridine diazine complex (6) is energetically lower than silver-bipyridine siloxy alkyne complex (7) in general even though the difference disappears based on the methodology. Thus, we have further taken the two possible reaction pathways into account.

We surmised that concerted and stepwise mechanisms may take place in the presence of Ag(I). Though we observed both synchronous and asynchronous concerted mechanism with the Ag(I)-ethylenediamine catalysis, we monitored only asynchronous with the Ag(I)-bipyridine. That also emphasizes the importance of the ligand which is used. However, no trace of stepwise mechanism was seen for both types of ligand but instead a single step product formation. The high asynchronicity was attributed to the asymmetric nature of the siloxy alkyne.

Beside the nucleophilic addition of siloxy alkyne to the complex 6, a nucleophilic attack of diazine to the complex 7 was considered as well. There was a considerable difference (~10 kcal/mol) between two resultant activation energies (Figure 5.7). Thus, we continued the scope of the catalyzed IEDDA of 1,2-diazine and siloxy alkyne by pursuing the former pathway.

In order to ensure the regioselectivity, we analyzed the Mulliken and NPA charges (Table 5.3 and Table 5.4) of the species and chose the transition structure (TSA) with the lower activation energy.

We were in accordance with the experimental data that assistance of Ag(I) gave ready access to the cycloaddition of 1,2-diazine and siloxy alkyne by lowering the activation barriers about 7-8 kcal/mol. The employed methodology has a significant effect in reflecting the pattern between TSA and TSB in terms of activation energies. The B3LYP results were useful in accordance with the qualitative analysis, however, produced unrealistic barriers impossible to overcome at room temperature. Accounting for kinetic density included in MPW1K functional improved the barriers and substitution of the obtained activation energies both in gas phase and dichloromethane into the Eyring equation on the basis of a bimolecular reaction provided consistent results in terms of reaction times. M06-L and ωB97XD single point calculations within 6-311+G(d,p)|SDD basis set also gave more realistic barriers resembling the MPW1K, albeit a little higher. In summary, MPW1K proves the significance of kinetic density parameter in transition state calculations.

In addition to and Ag(I) catalyzed and uncatalyzed (TSA and TSB) reactions, Lewis acid influence (TSC) was also examined. At this point, we couldn't get agreement with the experimental data which proposes the low yield of cycloadduct in the presence of any Lewis acid such as $SnCl_4$. Yet, the orbital analysis confirms the easy access of $SnCl_4$ catalyzed cycloaddition.

To ascertain the reproducibility of our methodology, we also modeled substituted 1,2-diazine and siloxy alkynes assisted by Ag(I) catalysis. In good agreement with the experiments, we reached higher activation energies in the case of dimethyl substituted diazine and methyl substituted siloxy alkyne (TSD and TSE) and a lower barrier for aryl substituted ethyl group introduced to the siloxy alkyne (TSF).

REFERENCES

1. Tsuchiya, Y. and Peter McCourt, "Strigolactones as Small Molecule Communicators", *Molecular Biosystems*, Vol. 8, pp. 464-469, 2012.

2. Dor, E., D. M. Joel, Y. Kapulnik, H. Koltai and J. Hershenhorn, "The Synthetic Strigolactone GR24 Influences the Growth Pattern Phytopathogenic Fungi", *Rapid Communication*, Vol. 234, pp. 419-427, 2011.

3. Rasmussen A., T. Heugebaert, C. Matthys, R. Van Deun, S. Goormachtiq, C. Stevens, D. Geleen, "A Fluorescent Alternative to the Synthetic Strigolactone GR24", *Molecular Plant*, Vol. 6, pp. 100-112, 2012.

4. Rasmussen, A., C. A. Beveridge, D. Geelen, "Inhibition of Strigolactones Promotes Adventitious Root Formation", *Plant Signaling and Behavior*, Vol. 7, pp. 694-697, 2012.

5. Zheng, J., K. Kwak, J. Xie and M. D. Fayer, "Ultrafast Carbon-Carbon Single-Bond Rotational Isomerization in Room-Temperature Solution", *Science*, Vol. 313, pp. 1951-1954, 2006.

6. Kuhn, R., *Molekulare Asymmetrie*, Stereochemie, Leipzig, Wien, 1933.

7. Ambrogi, M., A. Ciogli, M. Mancinelli, S. Ranieri and A. Mazzanti, "Atropisomers of Arylmaleimides: Stereodynamics and Stereodynamics and Absolute Configuration", *Journal of Organic Chemistry*, Vol. 78, pp. 3709-3719.

8. Sholl, D. S. and Janice A. Steckel, *Density Functional Theory*, Wiley, New Jersey, 2009.

9. Becke, A. D., "Density-Functional Exchange Energy Approximation with Correct Asymptotic Behavior", *Physical Review A*, Vol. 38, pp. 3098-3103, 1988.

10. Becke A. D., "A New Mixing of Hartree-Fock and Local Density Functional Theories", *Journal of Chemical Physics*, Vol. 38, pp. 1372-1377, 1993.

11. Parr, R. G. and W. Yang, *Density Functional Theory of Atoms and Molecules*, Oxford University Press, New York, 1989.

12. Handy, N. C., "Density Functional Theory", in: B. O. Roos ed., *Lecture Notes in Quantum Chemistry*, Vol. 2, pp. 91-123, Springer-Verlag, Berlin, 1994.

13. Leach, A. R., *Molecular Modeling Principles and Applications*, Prentice Hall, England, 2001.

14. Lee, C., W. Yang and R. G. Parr, "Development of Colle-Salvatti Correlation Energy Formula into a Functional of the Electron Density", *Physical Review B*, Vol. 37, pp. 785-789, 1988.

15. Becke, A. D., "Density Functional Thermochemistry. III. The Role of Exact Exchange", *Journal of Chemical Phys*ics, Vol. 98, pp. 5648-5652, 1993.

16. Pauling, L. J., "The Nature of the Chemical Bond. IV. The Energy of Single Bonds and the Relative Electronegativity of Atoms", *Journal of American Chemical Soc*iety, Vol. 54, pp. 3570-3582, 1932.

17. Tapia, O. and J. Bertrán, *Solvent Effects and Chemical Reactivity*, Kluwer Academic Publishers, The Netherlands, 1996.

18. Cramer, C. J. and D. G. Truhlar, "Implicit Solvation Models: Equilibria, Structure, Spectra, and Dynamics", *Chemical Reviews*, Vol. 99, pp. 2162-2220, 1999.

19. Tomasi, J., B. Mennucci and R. Cammi, "Quantum Mechanical Continuum Solvation Models", *Chemical Reviews*, Vol. 105, pp. 2999-3093, 2005.

20. Barone, V., M. Cossi and J. Tomasi, "Geometry Optimization of Molecular Structures in Solution by the Polarizable Continuum Model", *Journal of Computational Chemistry*, Vol.19, pp. 404-417, 1998.

21. Barone, V. and M. Cossi, "Quantum Calculation of Molecular Energies and Energy Gradients in Solution by a Conductor Solvent Model", *Journal of Physical Chemistry A*, Vol. 102, pp. 1995-2001, 1998.

22. Gaussian 09, Revision A.1, M. J. Frisch, G. W. Trucks, H. B. Schlegel, G. E. Scuseria, M. A. Robb, J. R. Cheeseman, G. Scalmani, V. Barone, B. Mennucci, G. A. Petersson, H. Nakatsuji, M. Caricato, X. Li, H. P. Hratchian, A. F. Izmaylov, J. Bloino, G. Zheng, J. L. Sonnenberg, M. Hada, M. Ehara, K. Toyota, R. Fukuda, J. Hasegawa, M. Ishida, T. Nakajima, Y. Honda, O. Kitao, H. Nakai, T. Vreven, J. A. Montgomery, Jr., J. E. Peralta, F. Ogliaro, M. Bearpark, J. J. Heyd, E. Brothers, K. N. Kudin, V. N. Staroverov, R. Kobayashi, J. Normand, K. Raghavachari, A. Rendell, J. C. Burant, S. S. Iyengar, J. Tomasi, M. Cossi, N. Rega, J. M. Millam, M. Klene, J. E. Knox, J. B. Cross, V. Bakken, C. Adamo, J. Jaramillo, R. Gomperts, R. E. Stratmann, O. Yazyev, A. J. Austin, R. Cammi, C. Pomelli, J. W. Ochterski, R. L. Martin, K. Morokuma, V. G. Zakrzewski, G. A. Voth, P. Salvador, J. J. Dannenberg, S. Dapprich, A. D. Daniels, Ö. Farkas, J. B. Foresman, J. V. Ortiz, J. Cioslowski, and D. J. Fox, Gaussian, Inc., Wallingford CT, 2009.

23. Ramachandran, K. I., G. Deepa and K. Namboori, *Computational Chemistry and Molecular Modeling*, Springer-Verlag, Berlin, Heidelberg, 2008.

24. Cramer, C. J., *Essentials of Computational Chemistry*, 2nd ed., Wiley, New Jersey, 2004.

25. McQuarrie, D. A., J. D. Simon, *Physical Chemistry: A Molecular Approach*, University Science Books, Sausalito, California, 1997.

26. Atkins, P. W., J. De Paula, *Atkins' Physical Chemistry*, 8th ed., Oxford University Press, Oxford, New York, 2006.

27. Woodward, R. B. and R. Hoffmann, "The Conservation of Orbital Symmetry", Academic Press, New York, 1970.

28. Fleming, I., *Pericyclic Reactions*, Oxford University Press, New York, 1999.

29. Carey, F. A. and R. J. Sundberg, *Advanced Organic Chemistry*, Springer, Virginia, 2008.

30. Linder, M. and T. Brick, "Synergistic Activation of the Diels–Alder reaction by an Organic Catalyst and Substituents: A Computational Study", *Organic and Biomolecular Chem*istry, Vol. 7, pp. 1304-1311, 2009.

31. Bachmann, W. E. and N. C. Deno, "The Diels-Alder Reaction of 1-Vinylnaphthalene with α,β- and α,β,γ,δ-Unsaturated Acids and Derivatives", *Journal of American Chemical Society*, Vol. 71, pp. 3062-3072, 1949.

32. Houk, K. N., Y. T. Lin and F. K. Brown, "Evidence for the Concerted Mechanism of the Diels-Alder Reaction of Butadiene with Ethylene", *Journal of American Chemical Society*, Vol. 108, pp. 554-556, 1986.

33. Ölçüm-Çelebi, N., D. H. Ess, V. Aviyente and K. N. Houk, "Effect of Lewis Acid Catalysts on Diels-Alder and Hetero-Diels-Alder Cycloadditions Sharing a Common Transition State", *Journal of Organic Chemistry*, Vol. 73, pp. 7472-7480, 2008.

34. Ölçüm-Çelebi, N., A. Sanyal and V. Aviyente, "Understanding the Stereoselection Induced by Chiral Anthracene Templates in Diels-Alder

Cycloaddition: A DFT Study", *Journal of Organic Chemistry*, Vol. 74, pp. 2328-2336, 2009.

35. Oishi, E., N. Taido, K. Iwamoto, A. Miyashita and T. Higashino, "Condensed Pyridazines", *Chemical and Pharmaceutical Bulletin*, Vol. 35, pp. 2686-2693, 1987.

36. Anderson, E. D. and D. L. Boger, "Inverse Electron Demand Diels–Alder Reactions of 1,2,3-Triazines: Pronounced Substituent Effects on Reactivity and Cycloaddition Scope", *Journal of American Chemical Society*, Vol. 133, pp. 12285–12292, 2011.

37. Oishi, E., N. Taido, K. Iwamoto, A. Miyashita and T. Higashino, "Ring Transformation of Phthalazines into Napthalenes by Means of Inverse-Electron-Demand Diels-Alder Reaction", *Chemical and Pharmaceutical Bulletin*, Vol. 38, pp. 3268-3272, 1990.

38. Gruseck, U. and M. Heuschmann, "The Remarkable Reactivity of 2-alkylidene-imidazolidines in Inverse Diels-Alder Reactions", *Tetrahedron Letters*, Vol. 28, pp. 6027-6030, 1987.

39. Hilt, G. and J. Janikowski, "Regiocontrolled Cobalt-Catalyzed Diels-Alder Reactions of Silicon-Functionalized, Terminal, and Internal Alkynes", *Organic Letters*, Vol. 11, pp. 773-776, 2009.

40. Boger, D. L. and R. S. Coleman, "Intramolecular Diels-Alder reactions of 1,2-diazines: General Indoline Synthesis. Studies on the Preparation of the Central and Right-Hand Segment of CC-1065", *Journal of Organic Chemistry*, Vol. 49, pp. 2240-2245, 1984.

41. Boger, D. L. and S. M. Sakya, "Total Synthesis of Prodigiosin, Prodigiosene, and Desmethoxyprodigiosin: Diels-Alder Reactions of Heterocyclic Azadienes and Development of an Effective Palladium(II)-Promoted 2,2'-bipyrrole Coupling

Procedure", *Journal of Organic Chemistry*, Vol. 53, pp. 1405-1415, 1988.

42. Boger, D. L. and R. S. Coleman, "Diels-Alder Reactions of Heterocyclic Azadienes: Total Synthesis of PDE-I, PDE-II, and PDE-I Dimer Methyl Ester", *Journal of American Chemical Society*, Vol. 109, pp. 2717-2727, 1987.

43. Boger, D. L. and M. Zhang, "Total Synthesis of (.+-.)-cis and (.+-.)-trans-trikentrin A: Diels-Alder Reactions of Heteroaromatic Azadienes", *Journal of American Chemical Society*, Vol. 113, pp. 4230-4234, 1991.

44. Kessler, N. S. and H. A. Wegner, "Lewis Acid Catalyzed Inverse Electron-Demand Diels-Alder Reaction of 1,2-Diazines", *Organic Letters*, Vol. 12, pp. 4062-4065, 2010.

45. Lorbach, A., M. Bolte, H. W. Lerner and M. Wagner, "Lewis-Base Adducts of 9,10-dihydro-9,10-diboraanthracene: Ditopic Hydroboration Reagents and a B–N Analogue of Triptycene", *Chemical Communications*, Vol. 46, pp. 3592-3594, 2010.

46. Türkmen, E. Y., T. J. Montavon, S. A. Kozmin and V. H. Rawal, "Silver-Catalyzed Formal Inverse Electron-Demand Diels−Alder Reaction of 1,2-diazines and Siloxy Alkynes", *Journal of American Chemical Society*, Vol. 134, pp. 9062-9065, 2012.

47. Nicolou, K. C., S. A. Snyder, T. Montagnon and G. Vassilikogiannakis, "The Diels-Alder Reaction in Total Synthesis", *Angewandte Chemie*, Vol. 41, pp. 1668-1698, 2002.

48. Sweis, R. F., M. P. Schramm and S. A. Kozmin, "Silver Catalyzed [2+2] Cycloadditions of Siloxy Alkynes", *Journal of American Chemical Society*, Vol. 126, pp. 7442-7443, 2004.

49. Fan, T., X. Chen, J. Sun and Z. Lin, "DFT Studies on Gold-Catalyzed

Cycloisomerization of 1,5-Enynes", *Organometallics*, Vol. 31, pp. 4221-4227, 2012.

50. Schultz, N. E., Y. Zhao and D. G. Truhlar, "Databases for Transition Element Bonding: Metal−Metal Bond Energies and Bond Lengths and Their Use to Test Hybrid, Hybrid Meta, and Meta Density Functionals and Generalized Gradient Approximations", *Journal of Physical Chemistry A*, Vol. 109, pp. 4388-4403, 2005.

51. Schultz, N. E., Y. Zhao and D. G. Truhlar, "Density Functionals for Inorganometallic and Organometallic Chemistry", *Journal of Physical Chemistry A*, Vol. 109, pp. 11127-11143, 2005.

52. Furche, F. and J. P. Perdew, "The Performance of Semi-Local and Hybrid Density Functionals in 3d Transition Metal Chemistry", *Journal of Chemical Physics*, Vol. 124, pp. 044103-0044130, 2006.

53. Cramer, C. J. and D. G. Truhlar, "Density Functional Theory for Transition Metals and Transition Metal Chemistry", *Physical Chemistry Chemical Physics*, Vol. 11, pp. 10757–10816, 2009.

54. Stephens, P. J., F. J. Devlin, C. F. Chabalowski and M. J. Frisch, "Ab Initio Calculation of Vibrational Absorption and Circular Dichroism Spectra Using Density Functional Force Fields", *Journal of Physical Chemistry*, Vol. 98, pp. 11623-11627, 1994.

55. Zhao, Y. and D. G. Truhlar, "The M06 Suite of Density Functionals for Main Group Thermochemistry, Kinetics, Noncovalent Interactions, Excited States, and Transition Elements: Two New Functionals and Systematic Testing of Four M06 Functionals and Twelve Other Functionals", *Theoretical Chemistry Accounts*, Vol. 120, pp. 215-241, 2008.

56. Zhao, Y. and D. G. Truhlar, "A New Local Density Functional for Main-Group

Thermochemistry, Transition Metal Bonding, Thermochemical Kinetics, and Noncovalent Interactions", *Journal of Chemical Physics*, Vol 125, pp.194101-194118, 2006.

57. Turro, N. J., *Modern Molecular Photochemistry*, University Science Books, Sausalito, 1991.

58. Zhao, Y. and D. G. Truhlar, "Density Functionals with Broad Applicability in Chemistry", *Accounts of Chemical Research*, Vol. 41, pp. 157-167, 2008.

59. Zhao, Y. and D. G. Truhlar, "Attractive Noncovalent Interactions in the Mechanism of Grubbs Second Generation Ru Catalysts for Olefin Metathesis", *Organic Letters*, Vol. 9, pp. 1967-1970, 2007.

60. Cramer, C. J., J. R. Gour, A. Kinal, M. Wloch, P. Piecuch, A. R. Shahi and L. Gagliardi, "Stereoelectronic Effects on Molecular Geometries and State-Energy Splittings of Ligated Monocopper Dioxygen Complexes", *Journal of Physical Chemistry A*, Vol. 112, pp. 3754-3767, 2008.

61. Savin, A., *Recent Developments and Applications of Modern Density Functional Theory*, ed. J. Seminario, Elsevier, New York, 1996.

62. Leininger, T., H. Stoll, H. J. Werner and A. Savin, "Combining Long-Range Configuration Interaction with Short-Range Density Functionals", *Chemical Physics Letters*, Vol. 275, pp. 151-160, 1997.

63. Iikura, H., T. Tsuneda, T. Yanai and K. Hirao, "A Long-Range Correction Scheme for Generalized-Gradient-Approximation Exchange Functionals", *Journal of Chemical Physics*, Vol. 115, pp.3540-3544, 2001.

64. Heyd, J. and G. E. Scuseria, "Assessment and Validation of a Screened Coulomb Hybrid Density Functional", *Journal of Chemical Physics*, Vol. 120, pp. 7274-7280, 2004.

65. Baer, R. and D. Neuhauser, “Density Functional Theory with Correct Long-Range Asymptotic Behavior”, *Physical Review Letters*, Vol. 94, pp. 043002-043005, 2005.

66. Livshitz, E. and R. Baer, “A Well-Tempered Density Functional Theory of Electrons in Molecules”, *Physical Chemistry Chemical Physics*, Vol. 9, pp. 2932-2941, 2007.

67. Henderson, T. M., A. F. Izmaylov, G. E. Scuseria and A. Savin, “The Importance of Middle-Range Hartree-Fock-Type Exchange for Hybrid Density Functionals”, *Journal of Chemical Physics*, Vol. 127, pp. 221103-221106, 2007.

68. Minenkov, Y., A. Singstad, G. Occhipintia and V. R. Jensen, “The Accuracy of DFT-Optimized Geometries of Functional Transition Metal Compounds: A Validation Study of Catalysts for Olefin Metathesis and Other Reactions in the Homogeneous Phase”, *Dalton Transactions*, Vol. 41, pp. 5526-5541, 2012.

69. Quintal, M., A. Karton, M. A. Iron, A. D. Boese and J. M. L. Martin, “Benchmark Study of DFT Functionals for Late-Transition-Metal Reactions”, *Journal of Physical Chemistry A*, Vol. 110, pp. 709-716, 2006.

70. Lynch, B. J., P.L. Fast, “Adiabatic Connection for Kinetics”, *Journal of Physical Chemistry A*, Vol. 104, pp. 4811-4815, 2000.

71. Dyall, K. G. and K. Faegri, *Introduction to Relativistic QuantumChemistry*, Oxford University Press, New York, USA, 2007.

72. Rösch, N., A. Matveev, V. A. Nasluzov, K. M. Neyman, L. Moskaleva and S. Kruger, *Relativistic Electronic Structure Theory*, Part 2. Applications, ed. P. Pyykko and P. Schwerdtfeger, Elsevier, Amsterdam, 2004.

73. Van Lenthe, E. and E. J. Baerends, "Optimized Slater-Type Basis Sets for the Elements 1-118", *Journal of Computational Chemistry*, Vol. 24, pp. 1142-1156, 2003.

74. Roos, B. O., R. Lindh,. P. A. Malmqvist, V. Veryazov and P. O. Widmark, "New Relativistic Ano Basis Sets for Transition Metal Atoms", *Journal of Physical Chemistry A*, Vol. 109, pp. 6575-6579, 2005.

75. Whitcomb, D. R. and R. D. Rogers, "The Properties, Crystals, and Molecular Structure Catena[μ-acetato-)(μ-phthalazine)silver(I)dihydrate]: $\{[Ag(\mu\text{-}O_2CCH_3)(\mu\text{-}PHZ)(H_2O_2)]_2\}_n$", *Journal of Chemical Crystallography.*, Vol. 25, pp. 137-141, 1995.

76. Whitcomb, D. R. and M. Rajeswaran, "Unusual Silver Coordination by Mono-Carboxylate Utilization of a Poly-Carboxylate Anion, Solid-State Structures of Silver-Tetrachlorophthalate with Phthalazine and Amine Ligands", *Inorganica Chimica Acta*, Vol. 361, pp. 1357-1362, 2008.